Tectonophysics 670 (2016) 1–15

Contents lists available at ScienceDirect

Tectonophysics

journal homepage: www.elsevier.com/locate/tecto

Review Article

Teleseismic constraints on the geological environment of deep episodic slow earthquakes in subduction zone forearcs: A review

Pascal Audet [a,*], YoungHee Kim [b,*]

[a] Department of Earth and Environmental Sciences, University of Ottawa, Ottawa, Canada
[b] School of Earth and Environmental Sciences, Seoul National University, Republic of Korea

ARTICLE INFO

Article history:
Received 26 August 2015
Received in revised form 8 January 2016
Accepted 9 January 2016
Available online 18 January 2016

Keywords:
Subduction zone
Slow earthquakes
Geologic structure
Teleseismic scattering

ABSTRACT

More than a decade after the discovery of deep episodic slow slip and tremor, or slow earthquakes, at subduction zones, much research has been carried out to investigate the structural and seismic properties of the environment in which they occur. Slow earthquakes generally occur on the megathrust fault some distance downdip of the great earthquake seismogenic zone in the vicinity of the mantle wedge corner, where three major structural elements are in contact: the subducting oceanic crust, the overriding forearc crust and the continental mantle. In this region, thermo-petrological models predict significant fluid production from the dehydrating oceanic crust and mantle due to prograde metamorphic reactions, and their consumption by hydrating the mantle wedge. These fluids are expected to affect the dynamic stability of the megathrust fault and enable slow slip by increasing pore-fluid pressure and/or reducing friction in fault gouges. Resolving the fine-scale structure of the deep megathrust fault and the in situ distribution of fluids where slow earthquakes occur is challenging, and most advances have been made using teleseismic scattering techniques (e.g., receiver functions). In this paper we review the teleseismic structure of six well-studied subduction zones (three hot, i.e., Cascadia, southwest Japan, central Mexico, and three cool, i.e., Costa Rica, Alaska, and Hikurangi) that exhibit slow earthquake processes and discuss the evidence of structural and geological controls on the slow earthquake behavior. We conclude that changes in the mechanical properties of geological materials downdip of the seismogenic zone play a dominant role in controlling slow earthquake behavior, and that near-lithostatic pore-fluid pressures near the megathrust fault may be a necessary but insufficient condition for their occurrence.

Contents

* Corresponding authors.
E-mail addresses: pascal.audet@uottawa.ca (P. Audet), younghkim@snu.ac.kr (Y. Kim).

http://dx.doi.org/10.1016/j.tecto.2016.01.005
0040-1951/

1. Introduction

Subduction zone great earthquakes (with moment magnitude $M_w > 8$) are generated by rupture of the megathrust fault within the so-called "seismogenic zone". There are many ways of determining the seismogenic zone based on a variety of indicators. In a static association with physical properties, the seismogenic zone is the portion of the fault that behaves in a brittle fashion. The depth to a specific geotherm commonly dictates the extent of the zone beyond which rocks deform by thermally activated creep processes (e.g., Handy et al., 2007). The strength of the brittle zone depends on the coefficient of friction on the fault and the pore-fluid pressure around the fault zone. Dynamically, the seismogenic zone is associated with the "locked" portion of the plate boundary fault as constrained by GPS and other geodetic data and coincides with the unstable slip region of fault rupture under rate and state friction (e.g., Lay et al., 2012). The extent of the seismogenic zone and the transition from unstable to stable slip depends on material properties and pore-fluid pressure around the fault surface (e.g., Scholz, 1998). Knowledge of the extent, geometry and material properties of the megathrust fault zone is therefore crucial to constrain the static and dynamic conditions under which large potentially damaging subduction zone earthquakes occur.

The megathrust fault remains largely inaccessible to direct sampling, except for exhumed ancient subduction thrust faults (e.g., Meneghini et al., 2010; Angiboust et al., 2015) and rare instances of direct drilling into the upper part of the subduction thrust (e.g., Chester et al., 2013). We therefore generally rely on indirect measurements to constrain its structure and physical properties via remote geophysical methods. Recent large-scale, high-density seismic array data have been very successfully in imaging the seismic structure of the subduction zone forearc, such as the megathrust fault zone, oceanic Moho, and upper plate Moho using receiver functions. Detailed images from three-dimensional regional seismic tomography and interface reflection structure models also provide additional constraints on subduction zone properties.

In recent years our view of the seismogenic zone has been improved by the discovery of widespread episodic slow slip events that occur downdip of the seismogenic zone. Slow slip events (sometimes referred to as slow earthquakes) had been recognized for some time in the literature using strainmeters (Linde et al., 1996) and seismometers (e.g., Kanamori and Stewart, 1979), although their importance and locations only became apparent when networks of GPS stations started recording and documenting their widespread occurrence. Associated with slow slip, a new source of seismic energy (called non-volcanic tremor) in the forearc was discovered by Obara (2002) off southwest Japan, which appeared as coherent noise propagating across arrays of seismograph stations. Rogers and Dragert (2003) then found similar signals in the forearc of the Cascadia subduction zone that occurred concurrently with slow slip events and both phenomena recurred episodically, which led to the term "Episodic Tremor and Slip", or ETS. Although initial studies focused on subduction zones where young and warm plates are being subducted beneath a continental margin, episodic slow slip and/or tremor events were later recognized in various other subduction zones, in the shallow part of the megathrust fault near the trench (Saffer and Wallace, 2015, and references therein) as well as in the deeper parts of strike-slip faults (e.g., Nadeau and Dolenc, 2005). In this paper we refer to episodic slow fault rupture events (with either or both documented slow slip and tremor) as slow earthquakes, and focus on the main deep subduction zone slow earthquakes, i.e. those that happen at depths of 30 to 45 km usually along a large extent of the subduction zone.

These slow earthquakes display important characteristics that provide a deeper understanding of fault zone properties and dynamics. Slow slip events and tremor can be correlated both temporally and spatially (e.g., Cascadia and Japan, Bartlow et al., 2011; Hirose and Obara, 2010), or temporally only (e.g., Hikurangi, Yabe et al., 2014). It is possible to have observed slow slip without detectable tremor, and perhaps observed tremor without detectable slow slip (however, see Frank et al., 2015). Both deep slow slip and tremor generally occur near but downdip of the brittle–ductile transition, approximately coinciding with the transition from unstable to stable sliding in a region of conditional stability (e.g., Scholz, 1998; Fig. 1), although there may be a gap between the slow earthquake source region and the seismogenic zone in some cases (Hyndman et al., 2015). Their occurrence may be induced by fluid flow and fluid processes at the plate interface and within the overlying plate (Rubinstein et al., 2010, and references therein). Low frequency earthquakes (LFEs) have also been observed in coincidence with the slow slip and tremor in subduction zones, with focal mechanism and location consistent with interplate slip (Shelly et al., 2006, 2007). Recent seismic and numerical modeling results point to the contribution of elevated fluid pressure near the plate interface (Kodaira et al., 2004; Liu and Rice, 2007; Audet et al., 2009; Song et al., 2009). These findings are consistent with thermo-petrological models that predict significant fluid production in the vicinity of the slow earthquake source region from dehydration of the subducting oceanic crust (Hyndman and Peacock, 2003). Nevertheless, the variety of thermal and petrologic conditions across different subduction zones precludes a simple relation between slow earthquakes and the thermal state or dehydration stages in the subducting plate in which they occur (Peacock, 2009).

Several reviews on the observations of slow earthquakes have been published recently (Beroza and Ide, 2011; Gomberg et al., 2010; Rubinstein et al., 2010; Schwartz and Rokowski, 2007). In this review we focus on the structural and geological environment in which slow earthquakes occur as inferred primarily from teleseismic studies. In particular we examine structural properties of the slow earthquake source region at six well-studied subduction zones: Cascadia, Nankai, Mexico, Costa Rica, Alaska, and Hikurangi (Fig. 2). The first three are considered as "hot" subduction zones, i.e., for which the seismogenic zone is thermally controlled downdip before the mantle wedge corner, and the other three are cooler. We first define the forearc structural elements and describe their seismic properties based on thermo-petrological models of metamorphism. We then focus on subduction zone structure inferred from teleseismic scattering techniques and high-resolution tomographic studies for the six subduction zones. Lastly we discuss the controls that structure may have on slow earthquake behavior.

2. Seismic structure of the subduction zone forearc

Slow earthquakes in subduction zones generally occur at and near the interface between the subducting slab and the overlying crust and mantle wedge (Fig. 1). The slab-mantle interface downdip of the forearc mantle corner is composed of some combination of heterogeneously deformed oceanic crust and sedimentary cover juxtaposed with hydrated and metasomatized materials. Recent receiver function studies of the slab-mantle interface have identified zones of low seismic velocity and high P-to-S velocity ratio (Vp/Vs) at or near the top of the subducting lithosphere. Abers (2005) reported a 2–8 km thick, low-velocity channel at the top of the downgoing plate at various subduction regions, that has up to 14% slower P-wave velocity (Vp) at depths less than 150 km. These low-velocity features also extend updip where the slab is juxtaposed to continental crust and have been interpreted as extensively hydrated assemblages in the subducting lithosphere (Abers, 2005; Bostock, 2013). Such hydrated materials can promote aseismic behavior at depths greater than the forearc mantle corner (Peacock and Hyndman, 1999).

There are two sources of fluids in subduction forearcs: evolved pore waters as the pore structure collapses and metamorphic dehydration reactions with increasing temperature and pressure, the latter likely being more important at the depths of slow earthquakes (e.g., Peacock et al., 2011). The thermal structure of the subducting slab is therefore the main control on the production of metamorphic fluids. Fig. 3

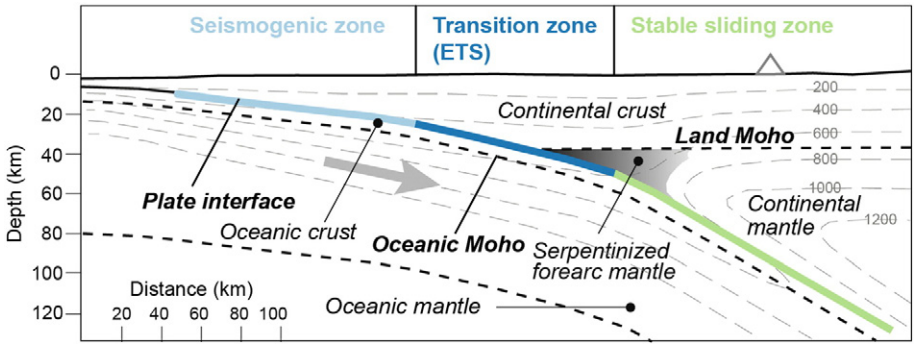

Fig. 1. Cross sectional schematic figure of slow earthquakes in the subduction zone, highlighting the seismogenic zone, transition zone, and stable sliding zone. The boundaries between these zones are approximate. Major structural elements are also highlighted: the oceanic crust and mantle, and continental crust and mantle. The gray shaded area shows the variably serpentinized mantle wedge corner. Slim gray dashed lines represent approximate isotherms (200 °C labels) and show the cooling effect of the slab on mantle wedge temperatures. The gray triangle shows the location of the volcanic arc. Figure modified from Peacock et al. (2011).

shows the pressure–temperature (P–T) of the subducted oceanic crust for the six subduction zones, from Syracuse et al. (2010), superimposed on metamorphic dehydration reactions of the subducted oceanic crust from Peacock and Wang (1999). We selected the P–T paths calculated for the case where the mechanical decoupling between the slab and the overriding plate occurs where slab temperature reaches 550 °C (see also Wada et al., 2008). These curves were obtained for subduction zone segments that may not reflect local conditions such as a lateral change in temperature regime along strike (e.g., Costa Rica, Hikurangi and Alaska). The main dehydration reaction is from hydrated metabasalts to the lower water content minerals of the eclogite field, which is accompanied by a large volume reduction and increase in rock density. Eclogite is also characterized by the highest seismic velocities among crustal rocks, similar to olivine-rich dunite (Christensen, 1996). An abrupt increase in the seismic velocity of subducting oceanic crust is taken to indicate the onset of eclogitization (Bostock et al., 2002; Rondenay et al., 2008), and the locus of peak fluid production. For Cascadia, Hyndman and Peacock (2003) calculated a fluid production of ~10^{-4} $m^3/(m^2\ yr)$ from the dehydration of the oceanic crust at 35 km depth near the slow earthquake source region, and a similar amount is expected from the dehydration of partially serpentinized uppermost mantle (Peacock et al., 2011), which amounts to about one teacup per square meter per year.

This fluid may: 1) remain trapped in the pore space of the dehydrating material, inducing high pore-fluid pressures, or 2) be transported into the overlying depleted peridotitic mantle wedge to produce serpentinite, mainly antigorite and lizardite, with some talc (Bostock et al., 2002; Hyndman and Peacock, 2003). Rocks with elevated pore-fluid pressures are characterized by high *Vp*/*Vs* values (which can also be expressed as high Poisson's ratios), much higher than rocks at dry conditions (Christensen, 1984). Fig. 4a shows *Vp*/*Vs* values measured in the laboratory at 1 GPa for various dry igneous and metamorphic rocks that are expected in a shallow (<45 km) subduction environment. Among these, lizardite has the highest *Vp*/*Vs* (2.1); most other rock types have *Vp*/*Vs* varying between 1.75 and 1.85. Fig. 4b shows laboratory measurements of *Vp*/*Vs* on a granite sample as a function of increasing confining pressure and pore-fluid pressure. These results show that elevated *Vp*/*Vs* values are obtained for rocks

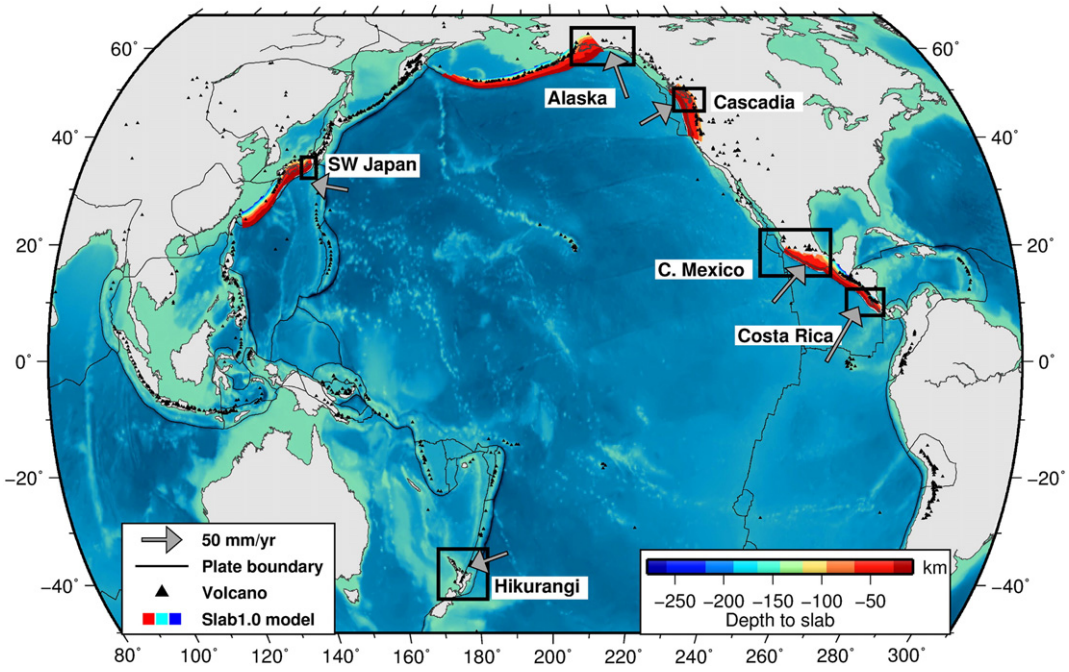

Fig. 2. Global map of selected subduction zones. Slab geometry models are indicated by the colors in the inset. The subduction geometries are from Slab1.0 (Hayes et al., 2012), and plate boundary from Bird (2003). Black boxes indicate regions for which individual seismic images are shown in Figs 5–10.

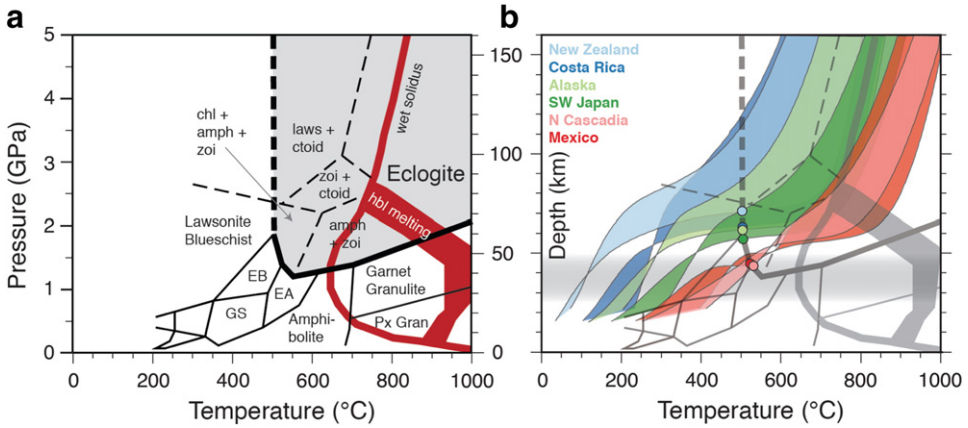

Fig. 3. Pressure–temperature (P–T) conditions of subducting oceanic crust. a. Metamorphic facies of meta-basaltic (EA, epidote–amphibolite; EB, epidote blueschist; GS, greenschist; Px Gran, pyroxene granulite) and eclogitic (amph, amphibole; ctoid, chlorotoid; laws, lawsonite; zoi, zoisite) oceanic crust (Peacock and Wang, 1999). Eclogite facies are shaded in light gray, and partial melting reactions for basaltic compositions in dark red. b. Calculated P–T paths and metamorphic assemblages encountered by subducting oceanic crust in six subduction zones (Syracuse et al., 2010). Colored bands show P–T path between top and bottom of oceanic crust; colored dots show P–T values where the oceanic crust enters the eclogite field. Although the range of P–T paths varies widely, most paths cross the basalt-to-eclogite reaction at ~500 °C within a depth range of 40 to 65 km. Gray shaded area indicates the depth range of deep slow earthquakes in most subduction zones. Figure modified from Peacock and Wang (1999).

characterized by very high pore-fluid pressure, independent of confining pressure. Fluid transport into the mantle wedge and the production of serpentinites also strongly affects seismic velocities. These metamorphic rocks have seismic velocities significantly lower than the peridotite protolith ($\delta Vs \approx -2$ km/s) or similar to mafic lower crustal rocks ($\delta Vs \approx 1$ km/s). Low inferred seismic velocities in the mantle wedge thus indicate serpentinite-rich material. Most of these minerals are also highly anisotropic, which complicates interpretation of isotropic velocity models but can provide important additional information on specific mineral abundances (e.g., Nikulin et al., 2009, Song and Kim, 2012, Piana Agostinetti and Miller, 2014).

Constraining the quantity of H_2O from downdip changes in seismic velocities of subducting material is therefore an important goal in studies of slow earthquake processes. In the following section we provide an overview of the constraints on the geologic environment of subduction zone forearcs from teleseismic scattering techniques that have been extensively studied in this regard. We note that teleseismic scattering data (i.e., receiver functions) are mainly sensitive to shear-wave impedance contrasts and velocity ratios; absolute velocities are more difficult to constrain.

3. Global survey

3.1. Cascadia

The Cascadia subduction zone extends from northern California in the south to northern Vancouver Island in the north where the Juan de Fuca plate subducts beneath the North American plate; here we mainly focus on its northern extent (Fig. 5a). The forearc of the Cascadia subduction zone has been extensively studied from active and passive source surveys (e.g., Green et al., 1986; Clowes et al., 1987; Soyer and Unsworth, 2006). Bostock (2013) provides a recent review of the structural elements as determined from teleseismic receiver function and other geophysical studies. Here we focus on structures in the vicinity of the slow earthquake source region.

The first studies of subduction zone structure from teleseismic receiver functions were carried out by Langston (1977, 1981) using a few broadband seismic stations in Oregon and British Columbia. Langston (1981) inferred the presence of a low-velocity zone that he interpreted as the crust of the subducting oceanic plate. Cassidy and Ellis (1993) corroborated these results using stations on northern

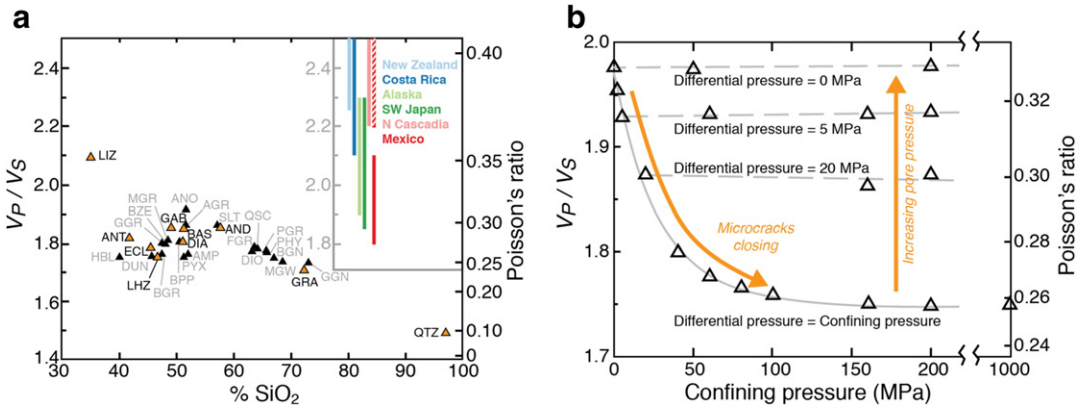

Fig. 4. Laboratory measurements of *Vp/Vs* values from Christensen (1984, 1996). a. *Vp/Vs* values for various rock samples measured at a confining pressure of 1.0 GPa plotted as a function of silica content. Selected samples are LIZ: Lizardite; ANT: Antigorite; GAB: Gabbro; BAS: Basalt; ECL: Eclogite; LHZ: Lherzolite; AND: Andesite; GRA: Granite; QTZ: Quartzite. Colored bars in the inset show the range of *Vp/Vs* values estimated from receiver functions (Audet et al., 2009; Audet and Bürgmann, 2014; Audet and Schwartz, 2013; Hansen et al., 2012; Kato et al., 2010; Kim et al., 2010, 2012, 2014). The red hatched bar indicates upper bounds from Audet and Bürgmann (2014) for Mexico. b. *Vp/Vs* measured on a granite sample as a function of confining pressure and pore-fluid pressure at undrained conditions and ambient temperature. Samples with high pore-fluid pressure (shown here as differential pressure = confining pressure − pore-fluid pressure) maintain high *Vp/Vs* values throughout the experiment. Figure modified from Peacock et al. (2011).

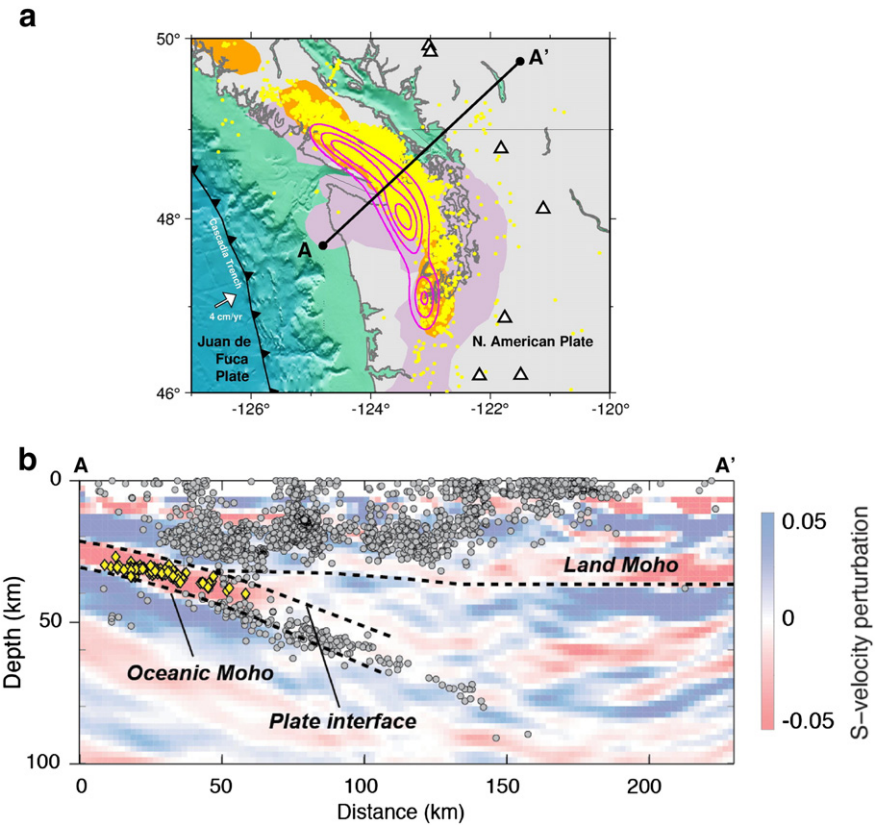

Fig. 5. Teleseismic image for the northern Cascadia subduction zone. a. Profile location (A–A'), slow slip events (34 events) highlighted as light purple region (Szeliga et al., 2008) and magenta contours (Gomberg et al., 2010), LFE zones in orange (Kao et al., 2009; Gomberg et al., 2010), and tremors (Idehara et al., 2014) in yellow dots. b. Teleseismic migration image (Nicholson et al., 2005) along A–A' modified from Bostock et al., 2012. Colors denote perturbations to S-velocity (d*Vs*/*Vs*) needed to generate observed seismic wavefields. Seismicity from the Canadian National Earthquake Database and LFEs (Bostock et al., 2012) are shown as gray circles and yellow diamonds, respectively. Dashed lines indicate interpreted features from the image.

Vancouver Island. The most significant breakthrough happened with the deployment of the temporary IRIS-PASSCAL CASC93 seismic network in central Oregon that delivered high-resolution images of deep subduction zone structure (Nabelek et al., 1996; Rondenay et al., 2001). These and more recent data from profiles across the subduction zone (Nicholson et al., 2005; Abers et al., 2009) reveal the continuity of the low-velocity zone inferred by Langston (1981) extending from the coast to approximately the intersection of the subducting plate with the continental Moho, below which the signals become difficult to trace.

There are three main features in the seismic images of particular interest for this review. First, the ~4 ± 1 km-thick low-velocity zone appears to be sandwiched between two higher velocity layers (Fig. 5b), implying that the inferred oceanic crust is characterized by S-wave velocities (*Vs*) that are low compared to both the underlying layer (representing either the mafic gabbroic part of the oceanic crust or the upper mantle of the subducting plate) and the overlying material (presumably gabbroic basement of the continental crust). Second, the signature of the low-velocity zone disappears at approximately 45 km depth (Fig. 5b), coincident with the peak of hydrated meta-basalt to eclogite reaction inferred from P–T paths of the oceanic crust based on thermal modeling (Peacock, 2009). As stated in Section 2, the transformation of hydrated meta-basalts to eclogite increases the seismic velocities of the downgoing layer, which are similar to the surrounding mantle. This interpretation implies that free fluids are abundant at the mantle wedge corner of the subduction zone. Third, the absence of a seismically-observed continental Moho near the mantle-wedge corner (Fig. 5b) is interpreted as pervasive serpentinization of the forearc mantle wedge (mainly antigorite). These findings are consistent with electrical resistivity studies in the forearc of Cascadia (Soyer and Unsworth, 2006; McGary et al., 2014) and point to significant fluid circulation and storage in the subduction zone forearc (e.g., Rondenay et al., 2008, Nikulin et al., 2009).

The northern Cascadia subduction zone is where aseismic slow slip was discovered by Dragert et al. (2001) and Miller et al. (2002) using GPS data. Rogers and Dragert (2003) characterized the recurrence of aseismic slow slip in conjunction with non-volcanic tremor beneath southern Vancouver Island that firmly established the presence of slow episodic megathrust fault rupture downdip of the seismogenic zone. These so-called episodic tremor and slip (ETS) events were later found to occur all along Cascadia (Brudzinski and Allen, 2007) from the mapping of either or both slow slip and tremor (e.g., Kao et al., 2008, Szeliga et al., 2008, Wech et al., 2009). At the time the lack of precise tremor hypocenters fuelled the debate regarding the nature of the tremor signal, whether it was occurring within the overriding plate as the slow slip was progressing and changing the stress field to generate hydraulic fracturing (Rogers and Dragert, 2003; Kao et al., 2005), or via direct shear slip on the plate interface during slow slip (Shelly et al., 2006, 2007). Low Frequency earthquakes (LFE) families that form at least part of the tremor during slow slip have now been found all along the Cascadia margin (Royer and Bostock, 2014; Plourde et al., 2015; Thomas and Bostock, 2015) and are consistent with shear slip on the plate interface (see also Rubin and Armbruster, 2013; Armbruster et al., 2014, for tremor locations). Interestingly, the location of LFE epicenters and inferred slow slip regions appears to coincide with the low-velocity signature inferred to be the downgoing oceanic crust (e.g., Audet et al., 2010; Bostock et al., 2012, Fig. 5b), suggesting that ETS may be related to deep fluid generation. Using teleseismic receiver

functions, Audet et al. (2009) and Hansen et al. (2012) resolved an extremely high *Vp*/*Vs* (2.35 ± 0.1) within the downgoing low-velocity zone around the slow earthquake source region (Fig. 4a, inset), interpreted as near-lithostatic pore-fluid pressure based on rock physical properties measured in the laboratory (Christensen, 1984, 1996). The updip edge of the main ETS zone also appears to be located approximately 70 km downdip of the seismogenic zone and around the mantle wedge corner (Hyndman et al., 2015), which suggests that fluids rising above the forearc mantle corner and along the plate interface may be responsible for ETS.

3.2. Southwest Japan

In southwest Japan the young and warm Philippine Sea plate subducts beneath the Eurasian plate (Fig. 6a). Following the 1995 Kobe earthquake, the National Research Institute for Earth Sciences and Disaster Prevention established the high-sensitivity seismograph network (Hi-net), composed of 600 borehole seismic stations in Japan. These high-quality data allowed the cataloging of LFEs by the Japan Meteorological Agency since 1999. In a milestone study, Obara (2002) studied high-frequency (1–8 Hz) continuous data temporally linked with the LFEs and discovered deep, long duration and long period tremor occurring along a narrow band of seismicity following the 35 to 40 km plate interface contour and near the intersection of the Philippine Sea plate with the mantle wedge corner, suggesting a link with the slab dehydration processes as discussed earlier. Since this discovery, several slow earthquake locations in southwest Japan have been described, each with its own frequency content, duration, recurrence interval and hypocentral location, some shallower than the main band of ETS. Obara (2011) provided a recent review of these various processes as well as their mutual interactions.

The high quality and density of seismic instrumentation in Japan have allowed detailed seismic velocity models. Particularly relevant for this review, Kodaira et al. (2004) provided a seismic tomographic velocity image showing a link between episodic slow slip and a dipping zone with high Poisson's ratio, exceeding 0.34 (*Vp*/*Vs* of ~2.1), interpreted as the subducting oceanic crust of the Philippine Sea plate at the northeast end of the Nankai trough with high pore-fluid pressure. Shelly et al. (2006) used LFEs within tremor in Shikoku in a tomographic inversion and confirmed the spatial correspondence between deep tremor and the zone of inferred high pore-fluid pressure (*Vp*/*Vs* ~1.9–1.95). Using receiver functions, Shiomi and Park (2008) determined the azimuth, dip angle and depth of the slab Moho beneath the Kii Peninsula, and found that the dip angle of the slab Moho becomes steeper downdip of the tremor source region, which they interpreted as a consequence of dehydration and transformation from basalt to high density eclogite within the subducting oceanic crust. Kato et al. (2010) used linear seismic array data along the onshore profile of Kodaira et al. (2004) (Fig. 6a), and provided a strong spatial correlation between the occurrence of the slow-slip event and LFEs, and zones of high-pressure fluids near the plate interface. Tremors appear to occur along the slab-mantle interface above the zone with moderately high *Vp*/*Vs* (~1.85) (Figs. 4a, inset, and 6b; Kato et al., 2010). Kitajima and Saffer (2012) reported inferred excess pore pressures (17–89 MPa) and low

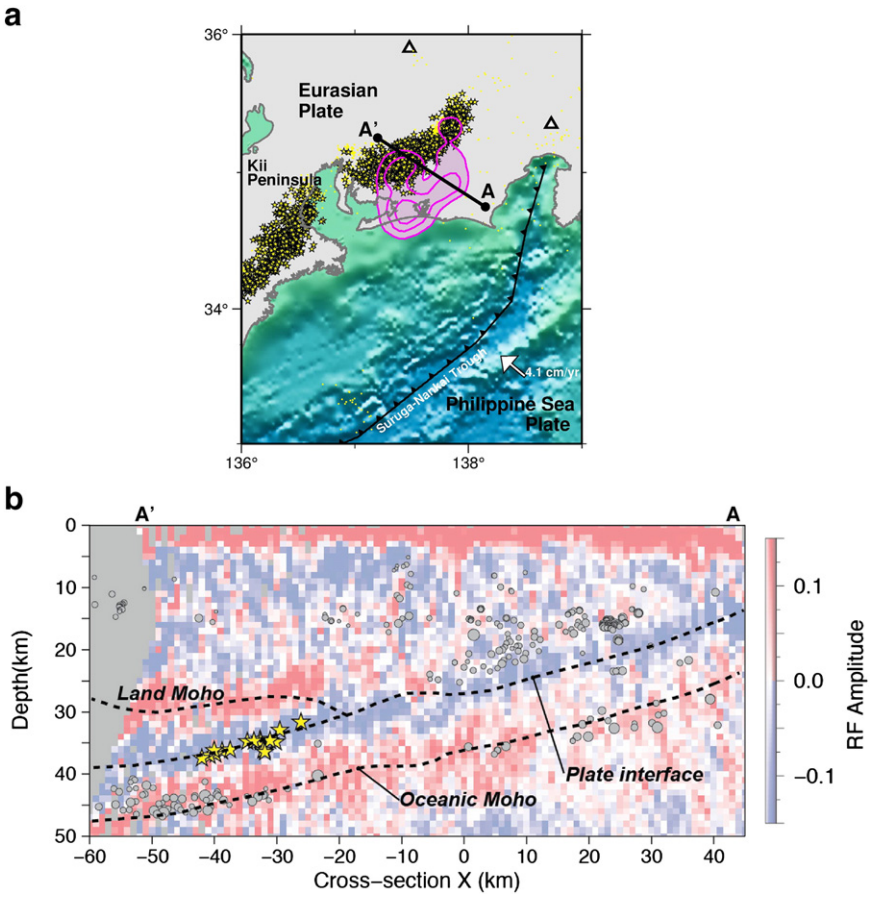

Fig. 6. Teleseismic image for the southwest Japan subduction zone. a. Profile location (A–A'), slow slip events highlighted as light purple region and magenta contours (Miyazaki et al., 2006), LFEs in yellow stars (reported by Japan Meteorological Agency), and tremors (Idehara et al., 2014) in yellow dots. b. Receiver function image along A–A' modified from Kato et al., 2010. Blue color indicates a negative impedance contrast across the velocity discontinuity whereas red color represents a positive impedance contrast. Relocated earthquakes and LFEs (Kato et al., 2010) are shown as gray circles and yellow stars, respectively.

effective stresses in the region offshore Kii Peninsula where LFEs have been identified (Ito and Obara, 2006), which supports the direct link between LFEs and low effective stress and high pore pressure.

3.3. Central Mexico

On the West Coast of central Mexico the Cocos plate is subducting beneath the North American plate along the Middle America Trench from the Tehuantepec Ridge in the southeast to the junction with the oceanic Rivera plate toward the northwest (Fig. 7a). Recent geophysical observations in central Mexico from dense seismic and GPS network data show that: 1) the plate interface dip shallows to nearly horizontal 150–300 km from the trench at a depth of ~45 km (Fig. 7b; Kim et al., 2010, 2012; Perez-Campos et al., 2008); and 2) from the geodetic data there is almost no tectonic or interseismic coupling between the two plates along the flat slab portion (Larson et al., 2004).

Aseismic slow slip events along the Mexican subduction zone were discovered shortly after Cascadia (Lowry et al., 2001); the results highlighted differences in slip duration and estimated seismic moment (Kostoglodov et al., 2003). Subsequent studies showed a variety of slow slip behavior, in particular long-term (~1 year) slow-slip events (Larson et al., 2007; Kostoglodov et al., 2010; Vergnolle et al., 2010; Radiguet et al., 2011) and non-volcanic tremors and LFEs (Payero et al., 2008; Husker et al., 2012; Frank et al., 2013, 2014) at a depth of 40–45 km near the plate interface (Fig. 7b, colored points). The greatest concentration of slow-slip displacement has been located just downdip of the seismogenic zone, based on thermal models (Fig. 7b, thick yellow line; Kostoglodov et al., 2010). Non-volcanic tremors occur in two distinct regions above the flat slab (Fig. 7b; Frank et al., 2014). Some tremors are triggered by transient stresses induced by teleseismic earthquakes and occur with the slow-slip events at or near the region where the slab geometry turns flat (Frank et al., 2013, 2014). Approximately 50 km farther downdip, the tremors occur more or less continuously, and are observed over a relatively shorter time period (several days) (Frank et al., 2013, 2014).

The low *Vs* layer (denoted as "ultra-slow velocity layer" (USL) by Song et al., 2009) atop the subducted Cocos crust appears to be in direct contact with overlying continental crust material (Perez-Campos et al., 2008; Kim et al., 2010, 2012), and the seismic velocity variations along the plate interface outline the seaward (updip) and landward (downdip) limits of the seismogenic zone (Song and Kim, 2012). The updip region near the Pacific coast shows a smaller *Vs* contrast at the base of the overlying crust in the strongly-coupled (geodetically-locked) seismogenic zone, where megathrust earthquakes are mostly concentrated (Fig. 7b, gray circles). Such a contrast abruptly increases toward the northeast at the transition zone, where the slow-slip events predominantly occur and where there is an absence of large-magnitude thrust earthquakes. Beyond this frictional transition zone, and where strong dehydration is concluded to occur (Manea and Manea, 2011), anomalously low *Vs* (2.4–3.4 km/s) are observed below the continental crust within a 4 ± 1 km thick layer (Song et al., 2009; Kim et al., 2010) with high *Vp*/*Vs* (1.8–2.1; Kim et al., 2010; Fig. 4a, inset), interpreted as relict serpentinized mantle (Perez-Campos et al., 2008; Kim et al., 2013). The hydrous minerals talc and serpentine are proposed to explain extremely low *Vs* and high *Vp*/*Vs* (Kim et al., 2010, 2013). Husker et al. (2012) suggested that the local conditions (i.e., temperature, pressure, and fluid content) are adequate to continuously generate tremor in the flat slab portion.

Around the transition from seismogenic to slow slip, there is evidence for seismic anisotropy larger than 5% with the foliation plane oriented 20 ± 10 degrees steeper than the plate interface, which is consistent with crystallographic preferred orientation developed in S-C mylonites (Song and Kim, 2012). These results were interpreted in terms of a rheological transition from a brittle regime with hydrostatic pore-fluid pressure gradient updip to a semi-brittle regime within a mylonitic shear zone with near-lithostatic fluid pressures coincident with the source region of the slow-slip events (Song and Kim, 2012).

3.4. Costa Rica

The Nicoya Peninsula in northwestern Costa Rica is located along the Middle America Trench in a region of large lateral variations in the nature of the subducting plates (Fig. 8a) that affect the seismogenic behavior of the megathrust fault (Newman et al., 2002). In the northwest, the subducting plate is formed at the East Pacific Rise and the plate interface is mostly locked along the margin according to GPS data and experiences large infrequent earthquakes. To the southeast, the subducting plate is formed at the Cocos-Nazca spreading centre and the plate interface is partially locked and generates frequent slow slip events. These changes along the margin are thought to reflect the change in the orientation of fabric and inferred permeability structure of the oceanic plate, which controls fluid circulation and local heat flow, leading to small-scale differences in the thermal regime (Harris et al., 2010). Along-strike variation in permeability structure of the incoming plate may also affect the degree of plate hydration and the subsequent build-up of pore-fluid pressure at greater depth, which in turn affect the rheology and stability of the plate interface.

The Nicoya Peninsula experiences areas of large slow-slip events approximately every 2 years (Jiang et al., 2012), in two main areas located offshore (northwest coastal area) and onshore (in the southeast) (Fig. 8a). The onshore slow slip appears to be irregular and coincides with major tremor episodes (Walter et al., 2011). However, much of the tremor consists of short duration, minor episodes without geodetically detectable slip. Interestingly, tremor occurs in freely slipping regions where the plate interface is weakly coupled as inferred from GPS data, both updip and downdip of the seismogenic zone (Walter et al., 2011). LFEs are also found coincident with tremor and slow slip at the updip edge of the seismogenic zone (Walter et al., 2013), as well as outside of the main tremor-producing area, near the downdip extent of the seismogenic zone, below the mantle wedge corner (Fig. 8; Brown et al., 2009).

Seismic investigations of subduction zone forearc structure beneath the Nicoya Peninsula include those of DeShon and Schwartz (2004) and DeShon et al. (2006)(Fig. 8) who used P- and S-wave tomography models from regional earthquake data to infer widespread serpentinization of the forearc mantle, similar to findings in Cascadia. Unfortunately, such seismic tomography models are not as accurate as receiver functions in delineating sharp velocity contrasts and may not resolve a thin LVZ (Audet et al., 2009). The profile shown on Fig. 8 is therefore not directly comparable to other subduction zone profiles shown in this paper; however it gives insight into the extent of mantle wedge serpentinization. MacKenzie et al. (2010) used a dense array of broadband stations and receiver function inversion and found a low-velocity zone in the forearc. The station density did not allow the mapping of the LVZ where slow-slip occurs. Linkimer et al. (2010) used receiver functions to study the nature of crustal terranes from the simultaneous determinations of Moho depth and *Vp*/*Vs* of the overlying crust and found relatively high *Vp*/*Vs* (1.80–1.92) for the Nicoya Peninsula. Audet and Schwartz (2013) used receiver functions from an expanded network on the Nicoya Peninsula and showed that the dipping 4 ± 1 km-thick low-velocity zone is characterized by high *Vp*/*Vs* ($>2.4 \pm 0.3$) (Fig. 4a, inset) and inferred high pore-fluid pressures, similar to Cascadia. Interestingly, the *Vp*/*Vs* of the overriding forearc crust appears to increase from ~1.75 in the northwest to ~1.95 in the southeast. Such large differences are difficult to explain in terms of lithology due to the uniform surface geology along the peninsula. These variations are interpreted as a change in fluid content within the forearc crust due to variable dehydration of the incoming plate beneath Nicoya Peninsula. To the northwest, the colder plate formed at the East Pacific Rise may be characterized by high permeability, trench-parallel normal faults that allow fluids to migrate out of the

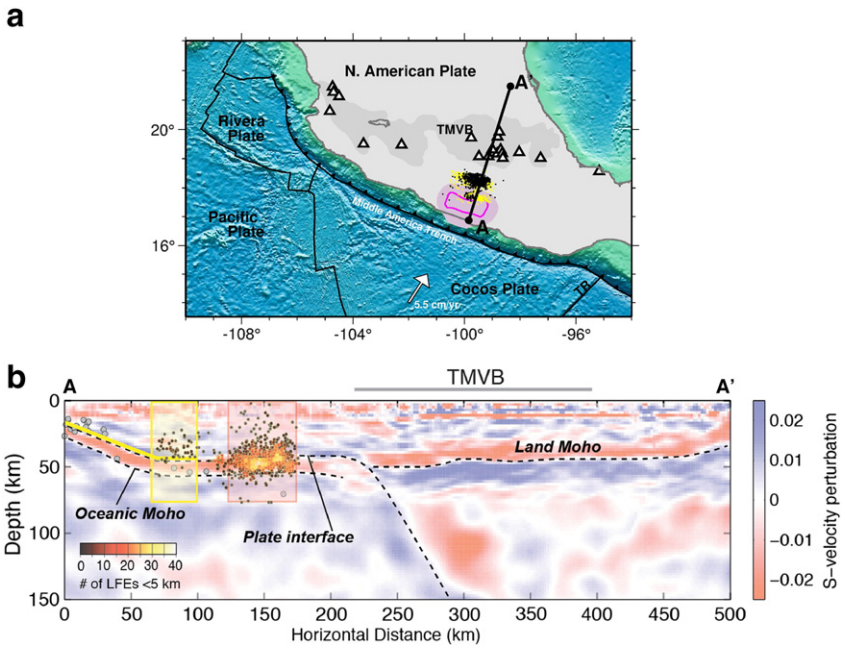

Fig. 7. Teleseismic image for the central Mexico subduction zone. a. Profile location (A–A'), slow slip events highlighted as light purple region and magenta contours (Yoshioka et al., 2004), LFEs in black dots (Frank et al., 2014) and tremors (Idehara et al., 2014) in yellow dots. b. Teleseismic migration image along A–A' modified from Kim et al., 2012. Colors denote perturbations to S-velocity (d*Vs*/*Vs*) needed to generate observed seismic wavefields. Relocated earthquakes (Pardo and Suarez, 1995) and 1120 LFEs are shown as gray circles and colored points, respectively (Frank et al., 2014). The orange and yellow boxes indicate the two LFE-active source regions: the yellow box is the region that was active during the large 2006 slow-slip event and is referred to as the transient zone; the orange box is the LFE/tremor sweet spot, where near-continuous LFE and tremor activity is observed. The thick yellow band above the subduction interface shows the calculated location of slip that occurred during the 2006 slow slip event (Kostoglodov et al., 2010). TMVB — Trans-Mexican Volcanic Belt. TR — Tehuantepec Ridge.

subduction zone efficiently. In the southeast, lower permeability and warmer temperatures of the subducting crust formed at the Cocos-Nazca spreading center may supply more fluids to the overriding plate. The lateral gradient in fluid content within the upper plate, increasing from northwest to southeast, may then decrease the strength and frictional resistance along the plate boundary and produce a lateral change in plate coupling, thus controlling the segmentation of seismogenic behavior, including slow slip and tremor.

On September 5, 2012, a magnitude M_w 7.6 earthquake ruptured a portion of the plate interface beneath the Nicoya Peninsula (Yue et al., 2013; Fig. 8a). Co-seismic slip models obtained using GPS and seismic data indicate that the rupture initiated offshore at a depth of 13 km, and migrated downdip to the intersection of the plate interface with the upper plate Moho, immediately updip of the deep LFE source region but within a tremor-producing area. The largest co-seismic large-slip patch overlaps a geodetically locked portion of the megathrust fault,

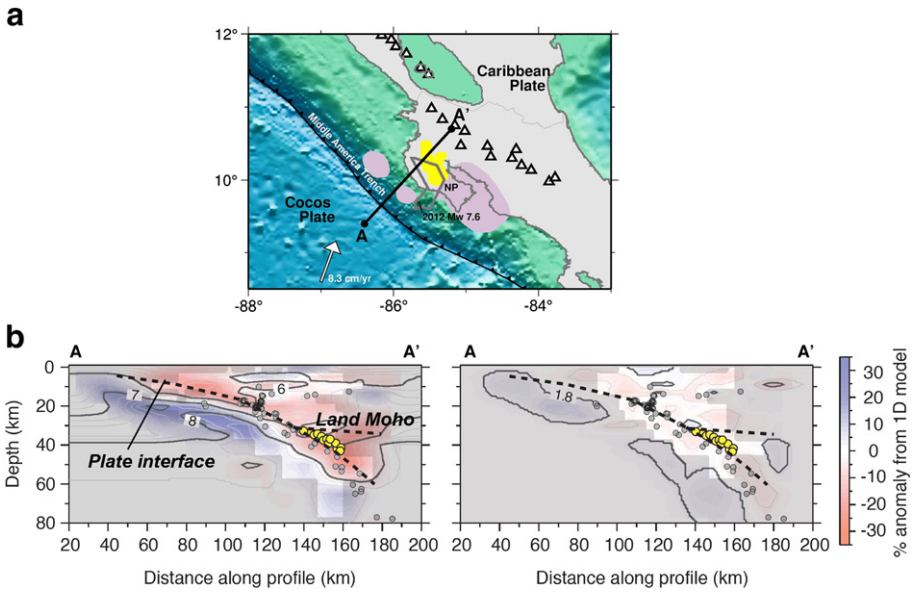

Fig. 8. Seismic image for the Costa Rica subduction zone. a. Profile location (A–A'), geodetic slow slip events highlighted as light purple region (Outerbridge et al., 2010), and LFEs in yellow (Brown et al., 2009). The 2012 Mw 7.6 earthquake rupture zone (Yue et al., 2013) is shown as gray contour. b. Tomography images along A–A' showing both P-wave (left) and *Vp*/*Vs* (right) anomalies relative to a 1-D velocity profile modified from DeShon et al., 2006. Gray-shaded area indicates more poorly resolved velocity model. Seismicity and LFEs (approximate location, from Brown et al., 2009) are shown as gray and yellow circles, approximately. NP — Nicoya Peninsula.

but does not extend into the main slow slip regions. Afterslip following the earthquake is bounded by the slow-slip area to the southeast, suggesting differences in frictional properties along strike (Malservisi et al., 2015) or that shear stress has been released in that area by slow slip. These results indicate a strong lateral variability in seismogenic zone properties that seem to correlate with subduction zone structure inferred from seismic and geophysical studies.

3.5. Alaska

The Alaska subduction margin exhibits east-to-west increases in subducting plate age and slab dip, and a decrease in slab temperature along the Aleutian trench, and is seismically active at a range of spatial and temporal scales. In particular, the tectonics of the easternmost part of the margin (Fig. 9a) are complex due to Yakutat and earlier terrane accretion since the Mesozoic (Plafker et al., 1994).

In the eastern Aleutian arc, an imaged, thin (3–5 km) low-velocity layer has ~20–40% slower *Vs* at the top interface of the Yakutat slab (~20–25 km depth) beneath the forearc continental crust (Fig. 9b). In this layer, *Vs* is estimated to be 2.0–2.5 km/s, which results in elevated *Vp*/*Vs* of 1.9–2.3 based on receiver function modeling (Kim et al., 2014; Fig. 4a, inset). The low-velocity anomalies at this depth may reflect properties of incoming, highly-sheared, fluid-saturated trench-fill sediments (von Huene et al., 1998; von Huene and Weinrebe, 2012). The subducting sedimentary column below the plate boundary is expected to have much slower (~10–30%) velocities than subducted oceanic crust lithologies. Alternatively, velocities at the top of the plate could be reduced by fluids in overpressured channels within or immediately below the plate interface. Elevated fluid pressures would arise from dehydration-produced fluids migrating upward, encountering permeability barriers along the thrust zone. In addition to high fluid pressure, crack anisotropy might contribute to such high *Vp*/*Vs* (exceeding 2.0; Wang et al., 2012).

Slow slip events in Alaska have been less well identified compared to those in the other subduction zones studied due to their long durations and long time intervals between the episodes. The scarcity of documented slow slip may express a different behavior under a cooler forearc environment, or it could reflect the limited availability of continuous geophysical data in the region. Slow slip occurs downdip of the seismogenic zone, defined here as the rupture zone of the 1964 earthquake (Ohta et al., 2006; Wei et al., 2012; Fig. 9a) and also represents a transition between completely locked and slipping segments of the plate interface inferred from GPS data (Zweck et al., 2002). Peterson and Christensen (2009) identified tremor signals on the downdip edge of the region with the highest slip during slow slip, approximately 50 km downdip of the seismogenic zone (Fig. 9a). The majority of the tremors that were observed after the onset of slow slip are bursts lasting between 10 and 15 min. Tremor depth estimates range widely over the region, partly due to inadequate station coverage (Peterson and Christensen, 2009). The source region of the slow slip and tremor coincides with the region where both seismic velocities and thickness of the thrust zone gradually increase with increasing metamorphic grade in the metasedimentary channel before the Yakutat slab subducts into the mantle beneath central Alaska (Kim et al., 2014; Fig. 9b). This region also roughly coincides with the mantle wedge corner, although this boundary is difficult to locate on the seismic image (Fig. 9b). Interestingly, the seismic signature of the LVZ extends within the rupture zone of the 1964 earthquake, updip of the slow slip source region.

Brown et al. (2013) identified tremor-like signals, composed of hundreds of LFEs along the Aleutian Trench, in four segments from east to west: Kodiak Island, Shumagin Gap, Unalaska, and Andreanof Islands. The LFE hypocenters along the arc are located at the downdip edge of the most recent large magnitude (M_w > 8.0) earthquakes (Brown

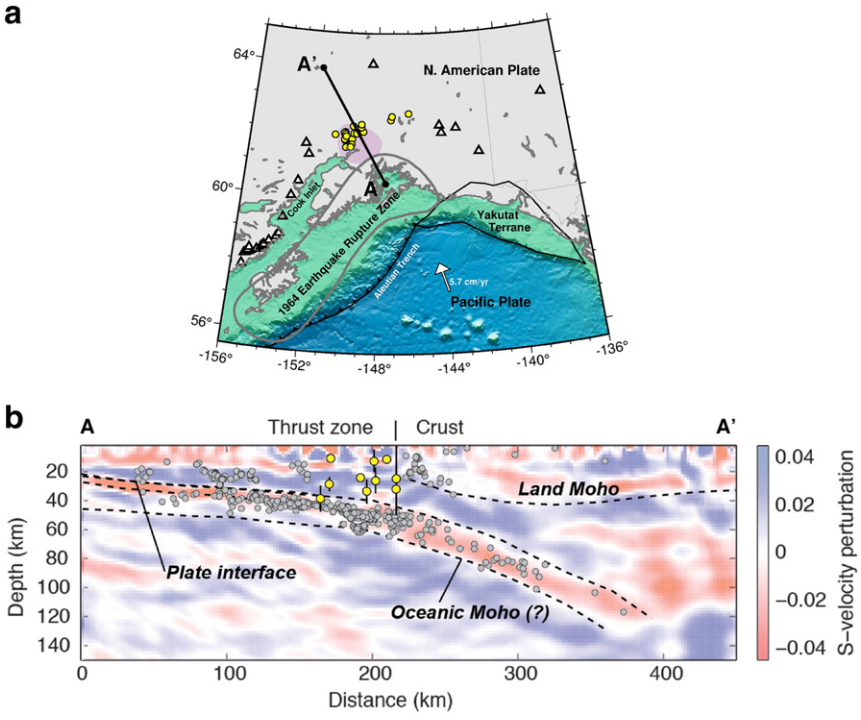

Fig. 9. Teleseismic image for the Alaska subduction zone. a. Profile location (A–A'), slow slip earthquakes highlighted as light purple region (Ohta et al., 2006), and non-volcanic tremors in yellow circles (Peterson and Christensen, 2009), which appear to occur at the region where the slab starts to dip steeply. The 1964 earthquake rupture zone (Zweck et al., 2002) is shown as gray contour. b. Teleseismic migration image along A–A' modified from Kim et al., 2014. Colors denote perturbations to S-velocity (d*Vs*/*Vs*) needed to generate observed seismic wavefields. Relocated earthquakes (Ferris et al., 2003; Li et al., 2013) and non-volcanic tremors (Peterson and Christensen, 2009) are plotted as gray and yellow circles, respectively. Uncertainty of the location of non-volcanic tremors is shown as a vertical bar. The top plate interface (horizontal distance of 0–380 km), the bottom interface of the thrust zone (0–180 km), and the bottom interface of Yakutat terrane (0–380 km) are denoted by dashed lines. The imaged thin red band (0–180 km) is very low-velocity megathrust zone, which sits at the top of the subducted Yakutat crust.

et al., 2013). Although their depth estimates are not well constrained, they suggest that the tremor activity marks the downdip rupture limit for great megathrust earthquakes in this subduction zone. These results indicate that tremors are also widespread in cold oceanic forearc environments.

3.6. Hikurangi

The Hikurangi margin, northern New Zealand, is characterized by subduction of the Hikurangi Plateau (Fig. 10a). Spatial variations in plate coupling at the Hikurangi subduction zone are well constrained by a dense network of geodetic stations, where full plate interface coupling based on GPS data occurs at shallow levels to the northeast, and extends to further depth to the southwest (Wallace et al., 2004). Slow slip events with a period of approximately two years have been detected downdip of the locked portion in both areas and follow a similar spatial pattern, with slow slip being much shallower to the northeast (Wallace and Beavan, 2010). Both long-term and short-term slow slip events occur along the Hikurangi margin. Recently, a slow slip event was detected in the deep portion of the plate interface at the central Hikurangi margin, at a depth similar to the slow slip occurring to the southwest (Wallace and Eberhart-Phillips, 2013), thus suggesting discontinuous coupling along both dip and strike. Tremor is found along the downdip edge of the deep slow slip events in the approximate vicinity of the mantle wedge corner (Fry et al., 2011; Ide, 2012), and is more elusive at shallower depths. Tremor activity associated with the 2010 slow-slip event is also identified to the northeast of the profile (Fig. 10a; Kim et al., 2011). The along-strike variations in the depth of deep slow slip events and tremor are taken to reflect lateral variations in the temperature of the plate interface based on modeling heat flow data (Yabe et al., 2014). In this region, the depth to the 350 °C and 600 °C isotherms, where deep slow slip and tremor originate, increases from 15 and 25 km in the northeast to 35 and 60 km in the southwest, respectively.

There is an abundance of high-resolution three-dimensional regional velocity models from P- and S-wave travel-time tomography studies (Reyners et al., 2006; Eberhart-Phillips and Reyners, 2012); in comparison, teleseismic scattering studies of the Hikurangi margin are sparse. Henrys et al. (2013) showed P-wave velocity structure of the forearc system from the active source data beneath the southern North Island. Bannister et al. (2007) used receiver functions to image subduction zone structure along a dense line of broadband stations running perpendicular to the trench, from Hawke's Bay to the backarc (Fig. 10a). The crust of the downgoing Hikurangi Plateau is imaged as a low-velocity zone that follows Wadati-Benioff seismicity, down to 60 km (Fig. 10b). Reyners et al. (2006) also observed a region with reduced velocities ($Vp < 8.0$ km/s) down to ~65 km depth along the similar profile region, and interpreted such feature as the subducted crust of the plateau. Eberhart-Phillips and Reyners (2012) documented velocity variations near the plate interface in the region southwest of the profile are closely related to the distribution of plate coupling (Wallace and Beavan, 2010). They suggested that the area of deep slow slip may correspond to zones of high pore-fluid pressure with elevated Vp/Vs above the slab. Observed lower Vp and higher Vp/Vs in the shallower slow slip region may indicate abundant fluid flux in forearc accretionary wedge (Eberhart-Phillips and Reyners, 2012).

Taken together, slow earthquake observations, thermal modeling and seismic velocity models indicate that temperature may be the main factor controlling the depth and lateral extent of the seismogenic zone at the Hikurangi margin (Yabe et al., 2014). In the northeast, the higher slab temperatures and fluid generation (with inferred high pore-fluid pressure) lower the depth to the brittle-ductile transition, as well as the depth of unstable to stable sliding, compared to the southwest. Importantly, tremors appear to occur at the downdip limit of the

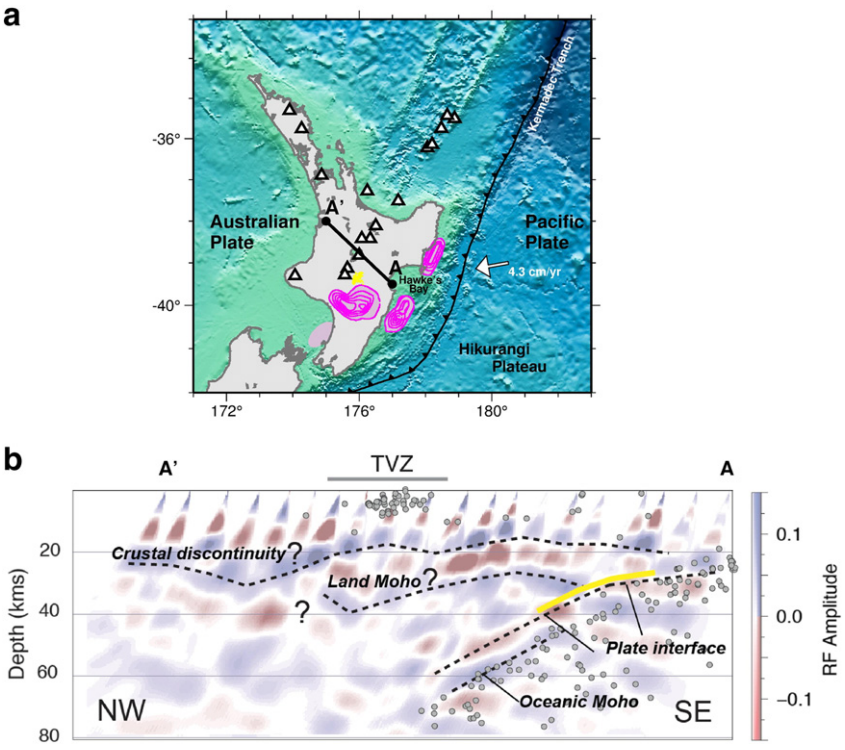

Fig. 10. Teleseismic image for the Hikurangi subduction zone. a. Profile location (A–A'), slow slip earthquakes highlighted as light purple region and magenta contours (McCaffrey et al., 2008), and tremors (Idehara et al., 2014) in yellow dots. b. Receiver function image along A–A' modified from Bannister et al., 2007. Note that colors are reversed from those in Fig. 6b: blue color indicates the positive impedance contrast across the velocity discontinuity whereas red color represents the negative impedance contrast. Specific discontinuities in seismic velocities (land Moho? crustal discontinuity?) are difficult to identify unambiguously from this image. Earthquakes are shown as circles. Yellow line highlights the location of SSE in central Hikurangi (Wallace and Eberhart-Phillips, 2013). TVZ — Taupo Volcanic Zone.

slow slip source region, where the plate interface is ~600 °C. These results suggest that slow earthquakes reflect the transient rheology of subducting material, controlled by variations in temperature and fluid generation along strike and dip, as opposed to the location of the mantle wedge corner.

4. Discussion

4.1. Structural controls on deep slow earthquake occurrence

There are at least two important features relating deep slow earthquake occurrence and the geologic structure across all subduction zones examined above. First, tremor and LFEs appear to occur near the top of the LVZ, whereas regular Wadati–Benioff seismicity is mostly restricted to the lower oceanic crust and upper mantle. Although tremor was originally thought to reflect hydrofracturing within the overlying continental crust (Kao et al., 2005), source mechanisms of repeating LFEs during tremor indicate that they represent shear slip on a fault (Shelly et al., 2007; Bostock et al., 2012). Second, deep ETS events occur downdip of the locked zone around the transition from unstable to stable slip, near the intersection of the downgoing plate with the overlying Moho and where the plate interface is ~30 to 40 km deep (Fig. 1). At least for Cascadia there is an apparent gap between the locked zone and the slow earthquake source region, perhaps reflecting a thermal control on the extent of the seismogenic zone for warm subduction zones.

The clustering of tremors and LFEs near the top of the LVZ suggests that it represents the deep extension of the megathrust fault or shear zone. The dipping LVZ observed in nearly all subduction zones worldwide is undoubtedly associated with material being entrained into the subduction zone (Vannucchi et al., 2012; Bostock, 2013). The exact nature of this material is debated, however, and has been interpreted either as some portion of the downgoing oceanic crust containing meta-basaltic rocks, subducted sediments, upthrusting serpentinite from the mantle wedge, or a tectonic "melange" composed of some or all of these elements and forming a thick shear zone (e.g., Vannucchi et al., 2012). This is an important question that needs to be resolved but is somewhat outside the scope of this review. Bostock (2013) recently compiled global observations of the LVZ and its depth extent and concluded that it represents the subducting, overpressured meta-basaltic oceanic crust (or some part thereof), but other models were considered as well.

More important for this review are the unusual properties (i.e., low seismic velocities, high *Vp*/*Vs* and Poisson's ratio) of the LVZ and its spatial correlation with the slow earthquake source region. It is often suggested that tremor occurrence is directly linked with the dehydration of the downgoing plate from prograde metamorphic reactions (Brantut et al., 2011; Fagereng and Diener, 2011). This is supported by the distribution of tremor signals around the transition from fluid-saturated meta-basalts to eclogitic rocks that peaks at roughly 40–45 km depth in northern Cascadia, southwest Japan and Mexico according to thermo-petrological models (Fig. 3; Peacock, 2009). However, a simple correspondence between the depth of tremor and the peak of eclogitization (or any particular metamorphic reaction or temperature regime (Peacock, 2009) does not hold for all subduction zones where deep slow earthquakes occur.

Regardless of the particular thermo-petrological conditions, the elevated *Vp*/*Vs* within the LVZ is likely to be related to pore-fluid pressures in excess of hydrostatic values (Fig. 4b), and may be close to lithostatic values (Christensen, 1984; Audet et al., 2009; Peacock et al., 2011). We note that elevated *Vp*/*Vs* obtained in these studies may in fact be biased due to the non-uniform sampling of highly anisotropic rocks (Wang et al., 2012). However the consistently high *Vp*/*Vs* values obtained at various subduction zones (Fig. 4a, inset) supports that the interpretation of excessive pore-fluid pressure is valid. These inferred high pore-fluid pressures have two main implications: 1) the effective normal stress acting on the plate boundary is very low, perhaps on the order of a few MPa (Kitajima and Saffer, 2012); and 2) their persistence as the oceanic plate reaches the continental Moho suggests the presence of a low-permeability plate boundary that prevents fluid migration into the overriding plate at the Myr time scale (Audet et al., 2009; Peacock et al., 2011). The low effective normal stresses are consistent with the triggering and modulation of tremor by small dynamic stresses such as passing surface waves (Rubinstein et al., 2007) and tidal stresses (Rubinstein et al., 2008; Royer et al., 2015), as well as numerical modeling of slow slip (Liu and Rice, 2007; Rubin, 2008; Segall et al., 2010). Based on the spatial correspondence between the LVZ and the slow earthquake source region, it is tempting to conjecture that high pore-fluid pressures inferred from elevated *Vp*/*Vs* values are responsible for deep episodic slow earthquake activity. However, regions of high *Vp*/*Vs* are not limited to the tremor producing area and extend both updip and downdip of this zone (Figs. 5–7, 9, 10). This suggests that near-lithostatic pore-fluid pressures may be a necessary but insufficient condition for slow earthquake occurrence.

As stated above, one implication of the LVZ characterized by high pore-fluid pressure is that the megathrust fault (or the top of the LVZ) is characterized by low vertical permeability. Indeed, maintaining near-lithostatic pore-fluid pressures necessarily implies that fluids do not easily flow upward to re-equilibrate along a hydrostatic pressure gradient. A plate boundary seal may be generated via a reduction in grain size due to shearing or mineral precipitation producing platy minerals such as clays. However, permeability is a dynamic and anisotropic property that varies over time scales of months to years and is temperature-dependent. Laboratory experiments show that bulk permeability of quartz gouges decrease exponentially at elevated pressures and temperatures following some perturbation (Giger et al., 2007). In a subduction zone, perturbations in the seal integrity may be generated by incremental volume changes due to prograde (or retrograde) metamorphic reactions, via hydro fracturing, or from mineral breakages during slow shear slip. Over the time scale of subduction (i.e., several Myrs), the fluids may flow or diffuse across the plate boundary and accumulate into the overlying plate and modify its structural and rheological properties. It is therefore apparent that slow earthquakes occur in a fluid-rich environment that likely controls the seismogenic properties of the megathrust fault.

The fate and redistribution of fluids at those depths is a matter of debate and depends primarily on the hydrological properties (porosity, permeability) of the various subduction zone elements as well as the stable mineral assemblages that produce or consume those fluids. Katayama et al. (2012) suggested that slow earthquakes might be linked with a contrast in permeability across the Moho above the subducting plate. In this model, slab-derived fluids are forced to flow toward the mantle wedge corner due to the extremely low permeability of the upper gabbroic layer just above the continental Moho, resulting in the local accumulation of fluids and the build-up of pore-fluid pressure. Serpentinites, in particular lizardite that is stable at low pressure and temperature conditions, incorporate significant amounts of water in their crystal structure, and may act to focus fluids near the mantle wedge corner in close proximity to the slow earthquake source region (Katayama et al., 2012). In a related but contrasting model, Hyndman et al. (2015) propose that the low permeability of sheared serpentinites blocks the vertical expulsion of fluids from the dehydrating oceanic crust and restricts flow along the plate interface. Upon reaching the mantle wedge corner, the fluids are released into the more permeable overlying forearc crust. This flux of fluids is inferred from low *Vp*/*Vs* values found above the mantle wedge corner within the overlying crust, which may be explained by the precipitation of silica into quartz veins. This model is also consistent with the bulk of tremor activity occurring near the mantle wedge corner in most subduction zones studied here (i.e., Cascadia, southwest Japan, Costa Rica and Alaska), producing a gap in seismogenic behavior of the megathrust as opposed to a smooth transition from unstable to stable sliding (Hyndman et al., 2015).

Alternatively, serpentinites (in particular antigorites) have much lower viscosity than that of major mantle-forming minerals and may be directly responsible for tremor generation via viscous relaxation of tectonic stresses (Hilairet et al., 2007). Finally, temperature may also directly affect the lateral and depth extent of the slow earthquake source region by controlling the depth to the brittle-ductile transition in a fluid-rich environment (Yabe et al., 2014). These models confirm a prominent role for metamorphic-derived fluids in the generation of slow earthquakes.

4.2. Structural controls on deep slow earthquake recurrence

Although a link between deep slow earthquakes and subduction zone structure and physical conditions has been established, the factors associated with variations in recurrence times remain poorly understood. Early attempts at explaining the periodicity of ETS appealed to modulation by periodic external forces including seasonal hydrologic loads (Lowry, 2006) and the Earth's 14-month pole tides (Shen et al., 2005). In the first case periodic slow fault slip may be a resonant response to small cyclical stress perturbations driven by climatic redistribution of the atmosphere, hydrosphere and cryosphere. These perturbations are largest near the coastline near the tremor source regions, may and modify the fault shear and normal stress to drive slow fault rupture during peak shear or peak slip-rate. In the second case, ETS periodicity may be related to pole-tide-induced stresses that modulate the stress field at the downdip edge of the seismogenic zone and may trigger slow fault rupture when conditions are favorable. In both cases, however, the large range of observed periods across different subduction zones (6 months to >2 years) and even across different segments (9 to 21 months in Cascadia) is difficult to reconcile with external, cyclical loads.

Alternative models invoke a role for the structure and geology of the subduction forearc environment in controlling or modulating the recurrence time of deep slow earthquakes. In Cascadia the segmentation of ETS along strike correlates qualitatively with the overriding forearc structure and geology, where the recurrence interval duration is inversely proportional to upper plate topography and spatially correlated with Bouguer gravity highs that were interpreted as megathrust asperities (Brudzinski and Allen, 2007). Wech and Creager (2011) compiled a tremor catalogue in northern Cascadia and found that the interval between tremor episodes and their duration decreases with increasing depth of the plate interface, suggesting that the megathrust fault weakens with depth. Using receiver function data, Audet and Bürgmann (2014) measured and compiled *Vp*/*Vs* (as a proxy for in-situ pore-fluid pressure) within the LVZ in six subduction zone forearcs and found that there is no correlation with tremor periodicity both at the global and local scale. Interestingly, there does seem to be a correlation between *Vp*/*Vs* of the overriding crust and tremor recurrence times. In northern Cascadia this is manifested as a decrease in forearc crust *Vp*/*Vs* with increasing depth to the plate interface, interpreted as a progressive enrichment in quartz content due to the strong temperature-dependent solubility of silica in slab-derived fluids (Manning, 1994) and its the precipitation into quartz veins into the upper continental crust (Hyndman et al., 2015). Such quartz enrichment requires significant amounts of silica-rich sediments that are entrained into the subduction zone. This observation suggests that temperature may be the main control on tremor periodicity via temperature-dependent permeability of quartz-rich fault gouge (Giger et al., 2007; Audet and Bürgmann, 2014).

5. Conclusions and future directions

Teleseismic scattering images of the various structural elements in subduction zone forearcs obtained from teleseismic scattering techniques provide constraints on the thermo-petrological environment of the deep extension of the megathrust fault. These images identify the distribution of inferred pore-fluid pressure and hydrated mineral assemblages and their potential effects on the stability of the megathrust fault in the slow earthquake source region. Fluids appear to facilitate slow slip through near-lithostatic pore-fluid pressures that reduce the effective normal stress and allow slip to occur at otherwise frictionally stable conditions. Slow slip may also be influenced by the contact of the fault with variably serpentinized mantle wedge, which controls the permeability of the system. Slow earthquake recurrence times correlate with the geology (i.e., *Vp*/*Vs*) of the overlying continental crust, thus reflecting either a direct control of bulk composition and strength on megathrust processes, or the dynamic control of temperature-dependent permeability on pore-pressure evolution via precipitation processes. Despite significant differences across the subduction zones examined here, we conclude that near-lithostatic pore-fluid pressures inferred from high *Vp*/*Vs* values are necessary for slow earthquakes to occur, but appear to be insufficient. These studies also point to both hydrologic and petrologic properties of the various subduction zone elements in determining where slow earthquakes occur. However, untangling these various effects is challenging and will require advances in multiple fields of research.

Avenues for future research linking slow earthquakes and the geology of subduction zone forearcs include numerical simulations of megathrust fault slip that incorporate material properties reflecting the petrology of the various structural elements to assess the role of rock composition in seismogenic processes (e.g., Liu and Rice, 2009). Ideally these models would incorporate realistic hydrological properties and fluid fluxes to make predictions that can be tested using seismic or other geophysical data. This effort will require laboratory measurements of rock properties in shear experiments at various hydrothermal conditions that reflect those of slow earthquake source regions.

Seismic investigations can also contribute to a deeper understanding of megathrust processes by increasing the resolution of seismic images and focusing on adjacent parts of the subduction zone forearc. For example, it will be important to use offshore seismic data to provide structural information of the incoming plate and conditions along the plate boundary interface from the trench through the seismogenic zone. Receiver function analysis using data from ocean bottom seismometers (OBS) from the Cascadia Initiative (Toomey et al., 2014) may be able to provide constraints on material properties and/or pore-fluid pressure around the (offshore) megathrust by tracing the up-dip extent of the low-velocity zone in Cascadia (Audet, 2015; Janiszewski and Abers, 2015).

Another promising avenue for seismic investigation is the characterization of seismic anisotropy around the slow earthquake source region (e.g., Song and Kim, 2012; Piana Agostinetti and Miller, 2014). Highly sheared rocks contain strong fabrics that provide information on the shearing process and the particular rock types involved. For instance, sheared serpentinites are highly anisotropic and this fabric influences the mechanical properties of the megathrust fault by favoring slip along weak planes (e.g., Faccenda et al., 2008; Katayama et al., 2009; Nikulin et al., 2009; Bezacier et al., 2010; Fagereng et al., 2010). Together with improved characterization and modeling of rock seismic properties (e.g., Cossette et al., 2015) from representative field samples, this line of work is likely to yield important insights into the effects of rock textures and fluids in understanding seismic images of subduction zone structures in the slow earthquake source region.

Acknowledgments

P. Audet is funded by the Natural Sciences and Engineering Research Council of Canada through grant RGPIN-418288-2012. Y. Kim is funded by the National Research Foundation of Korea Grant funded by the Korean Government (NRF-2014S1A2A2027609), and by the Korea Meteorological Administration Research and Development Program under Grant KMIPA2015-7020. The authors thank S. Bannister, M. Bostock, H. DeShon, W. Frank, A. Kato, and S. Ide for the data used in

figures, and two anonymous reviewers for comments that significantly improved this paper.

References

Abers, G.A., 2005. Seismic low-velocity layer at the top of subducting slabs: observations, predictions, and systematics. Phys. Earth Planet. Inter. 149, 7–29. http://dx.doi.org/10.1016/j.pepi.2004.10.002.

Abers, G.A., MacKenzie, L.S., Rondenay, S., Zhang, Z., Wech, A.G., Creager, K.C., 2009. Imaging the source region of Cascadia tremor and intermediate depth earthquakes. Geology 37, 1119–1122.

Angiboust, S., Kirsch, J., Oncken, O., Glodny, J., Monié, P., Rybacki, E., 2015. Probing the transition between seismically coupled and decoupled segments along an ancient subduction interface. Geochem. Geophys. Geosyst. 16, 1905–1922.

Armbruster, J.G., Kim, W.-Y., Rubin, A.M., 2014. Accurate tremor locations from coherent *S* and *P* waves. J. Geophys. Res. 119, 5000–5013. http://dx.doi.org/10.1002/2014JB011133.

Audet, P., 2015. Receiver functions using OBS data: Promises and limitations from numerical modelling and examples from the Cascadia Initiative. Geophys. J. Int. (in review).

Audet, P., Bürgmann, R., 2014. Possible control of subduction zone slow earthquake periodicity by silica enrichment. Nature 510, 389–392.

Audet, P., Schwartz, S.Y., 2013. Hydrologic control on forearc strength and seismicity in the Costa Rican subduction zone. Nat. Geosci. 6, 852–855.

Audet, P., Bostock, M.G., Boyarko, D.C., Brudzinski, M.R., Allen, R.M., 2010. Slab morphology in the Cascadia forearc and its relation to episodic tremor and slip. J. Geophys. Res. 115 (B00A16).

Audet, P., Bostock, M.G., Christensen, N.I., Peacock, S.M., 2009. Seismic evidence for overpressured subducted oceanic crust and megathrust fault sealing. Nature 457, 76–78.

Bannister, S., Reyners, M., Stuart, G., Savage, M., 2007. Imaging the Hikurangi subduction zone, New Zealand, using teleseismic receiver functions: crustal fluids above the forearc mantle wedge. Geophys. J. Int. 169, 602–616. http://dx.doi.org/10.1111/j.1365-246X.2007.03345.x.

Bartlow, N.M., Miyazaki, S., Bradley, A.M., Segall, P., 2011. Space–time correlation of slip and tremor during the 2009 Cascadia slow slip event. Geophys. Res. Lett. 38 (L18309). http://dx.doi.org/10.1029/2011GL048714.

Beroza, G.C., Ide, S., 2011. Slow earthquakes and nonvolcanic tremor. Annu. Rev. Earth Planet. Sci. 39, 271–296.

Bezacier, L., Reynard, B., Bass, J.D., Sanchez-Valle, C., Van de Moortèle, B., 2010. Elasticity of antigorite, seismic detection of serpentinites, and anisotropy in subduction zones. Earth Planet. Sci. Lett. 289, 198–208.

Bird, P., 2003. An updated digital model of plate boundaries. Geochem. Geophys. Geosyst. 4, 1027. http://dx.doi.org/10.1029/2001GC000252.

Bostock, M.G., 2013. The Moho in subduction zones. Tectonophysics 609, 547–557.

Bostock, M.G., Hyndman, R.D., Rondenay, S., Peacock, S.M., 2002. An inverted continental Moho and serpentinization of the forearc mantle. Nature 417, 536–538.

Bostock, M.G., Royer, A.A., Hearn, E.H., Peacock, S.M., 2012. Low frequency earthquakes below southern Vancouver Island. Geochem. Geophys. Geosyst. 13 (Q11007). http://dx.doi.org/10.1029/2012GC004391.

Brantut, N., Sulem, J., Schubnel, A., 2011. Effect of dehydration reactions on earthquake nucleation: stable sliding, slow transients, and unstable slip. J. Geophys. Res. 116 (B05304). http://dx.doi.org/10.1029/2010JB007876.

Brown, J.R., Beroza, G.C., Ide, S., Ohta, K., Shelly, D.R., Schwartz, S.Y., Rabbel, W., Thorwart, M., Kao, H., 2009. Deep low frequency earthquakes in tremor localize to the plate interface in multiple subduction zones. Geophys. Res. Lett. 36 (L19306).

Brown, J.R., Prejean, S.G., Beroza, G.C., Gomberg, J.S., Haeussler, P.J., 2013. Deep low-frequency earthquakes in tectonic tremor along the Alaska–Aleutian subduction zone. J. Geophys. Res. 118, 1079–1090. http://dx.doi.org/10.1029/2012JB009459.

Brudzinski, M.R., Allen, R.M., 2007. Segmentation in episodic tremor and slip all along Cascadia. Geology 35, 907–910.

Cassidy, J.F., Ellis, R.M., 1993. S-wave velocity structure of the northern Cascadia subduction zone. J. Geophys. Res. 98, 4407–4421.

Chester, F.M., Rowe, C.D., Ujiie, K., Kirkpatrick, J., Regalla, C., Remitti, F., Moore, J.C., Toy, V., Wolfson-Schwehr, M., Bose, S., Kameda, J., Mori, J.J., Brodsky, E., Eguchi, N., Toczko, S., Expedition 343, 343T Scientists, 2013. Structure and composition of the plate-boundary slip-zone for the 2011 Tohoku-oki earthquake. Science 342, 1208–1211.

Christensen, N.I., 1984. Pore pressure and oceanic crustal seismic structure. Geophys. J. R. Astron. Soc. 79, 411–423.

Christensen, N.I., 1996. Poisson's ratio and crustal seismology. J. Geophys. Res. 101, 3139–3156.

Clowes, R.M., Brandon, M.T., Green, A.G., Yorath, C.J., Sutherland Brown, A., Kanasewich, E.R., Spencer, C., 1987. LITHOPROBE southern Vancouver Island: Cenozoic subduction complex imaged by deep seismic reflections. Can. J. Earth Sci. 24, 31–51.

Cossette, E., Schneider, D.A., Audet, P., Graseman, B., Habler, G., 2015. Seismic properties and mineral crystallographic preferred orientations from EBSD data: results from a crustal-scale detachment system, Aegean region. Tectonophysics 651, 66–78.

DeShon, H.R., Schwartz, S.Y., 2004. Evidence for serpentinization of the forearc mantle wedge along the Nicoya Peninsula, Costa Rica. Geophys. Res. Lett. 31 (L21611).

DeShon, H.R., Schwartz, S.Y., Newman, A.V., Gonzalez, V., Protti, M., Dorman, L.M., Dixon, T.H., Sampson, D.E., Flueh, E.R., 2006. Seismogenic zone structure beneath the Nicoya Peninsula, Costa Rica, from three-dimensional local earthquake P- and S-wave tomography. Geophys. J. Int. 164, 109–124.

Dragert, H., Wang, K., James, T.S., 2001. A silent slip event on the deeper Cascadia subduction interface. Science 292, 1525–1528.

Eberhart-Phillips, D., Reyners, M., 2012. Imaging the Hikurangi Plate interface region, with improved local-earthquake tomography. Geophys. J. Int. 190, 1221–1242. http://dx.doi.org/10.1111/j.1365-246X.2012.05553.x.

Faccenda, M., Burlini, L., Gerya, T.V., Mainprice, D., 2008. Fault-induced seismic anisotropy by hydration in subducting oceanic plates. Nature 455, 1097–1100.

Fagereng, A., Diener, J.F.A., 2011. Non-volcanic tremor and discontinuous slab dehydration. Geophys. Res. Lett. 38 (L15302). http://dx.doi.org/10.1029/2011GL048214.

Fagereng, A., Remiti, F., Sibson, R.H., 2010. Shear veins observed within anisotropic fabric at high angles to the maximum compressive stress. Nat. Geosci. 3, 482–485.

Ferris, A., Abers, G.A., Christensen, D.H., Veenstra, E., 2003. High resolution image of the subducted Pacific (?) plate beneath central Alaska, 50–150 km depth. Earth Planet. Sci. Lett. 214, 575–588. http://dx.doi.org/10.1016/S0012-821X(03)00403-5.

Frank, W.B., Radiguet, M., Rousset, B., Shapiro, N.M., Husker, A.L., Kostoglodov, V., Cotte, N., Campillo, M., 2015. Uncovering the geodetic signature of silent slip through repeating earthquakes. Geophys. Res. Lett. 42, 2774–2779. http://dx.doi.org/10.1002/2015GL063685.

Frank, W.B., Shapiro, N.M., Husker, A.L., Kostoglodov, V., Romanenko, A., Campillo, M., 2014. Using systematically characterized low-frequency earthquakes as a fault probe in Guerrero, Mexico. J. Geophys. Res. 119, 7686–7700. http://dx.doi.org/10.1002/2014JB011457.

Frank, W.B., Shapiro, N.M., Kostoglodov, V., Husker, A.L., Campillo, M., Payero, J.S., Prieto, G.A., 2013. Low-frequency earthquakes in the Mexican sweet spot. Geophys. Res. Lett. 40, 2661–2666. http://dx.doi.org/10.1002/grl.50561.

Fry, B., Chao, K., Bannister, S., Peng, Z., Wallace, L., 2011. Deep tremor in New Zealand triggered by the 2010 *Mw* 8.8 Chile earthquake. Geophys. Res. Lett. 38 (L15306). http://dx.doi.org/10.1029/2011GL048319.

Giger, S.B., Tenthorey, E., Cox, S.F., Fitzgerald, J.D., 2007. Permeability evolution in quartz gouges under hydrothermal conditions. J. Geophys. Res. 112, B07202.

Gomberg, J., the Cascadia, Beyond Working Group., 2010. Slow-slip phenomena in Cascadia from 2007 and beyond: a review. Geol. Soc. Am. Bull. 122, 963–978.

Green, A.G., Clowes, R.M., Yorath, C.J., Spencer, C., Kanasewich, E.R., Brandon, M.T., Sutherland Brown, A., 1986. Seismic reflection imaging of the Juan de Fuca plate. Nature 319, 210–213.

Handy, M.R., Hirth, G., Hovius, N. (Eds.), 2007. Tectonic Faults: Agents of Change on a Dynamic Earth, MIT Press. Mass, Cambridge.

Hansen, R.T.J., Bostock, M.G., Christensen, N.I., 2012. Nature of the low velocity zone in Cascadia from receiver function waveform inversion. Earth Planet. Sci. Lett. 337–338, 25–38.

Harris, R.N., Spinelli, G., Ranero, C.R., Grevemeyer, I., Villinger, H., Barckhausen, U., 2010. Thermal regime of the Costa Rican convergent margin: 2. Thermal models of the shallow Middle America subduction zone offshore Costa Rica. Geochem. Geophys. Geosyst. 11 (Q12S29).

Hayes, G.P., Wald, D.J., Johnson, R.L., 2012. Slab1.0: a three-dimensional model of global subduction zone geometries. J. Geophys. Res. 117 (B01302). http://dx.doi.org/10.1029/2011JB008524.

Henrys, S., Wech, A., Sutherland, R., Stern, T., Savage, M., Sato, H., Mochizuki, K., Iwasaki, T., Okaya, D., Seward, A., Tozer, B., Townend, J., Kurashimo, E., Iidaka, T., Ishiyama, T., 2013. SAHKE geophysical transect reveals crustal and subduction zone structure at the southern Hikurangi margin, New Zealand. Geochem. Geophys. Geosyst. 14, 7. http://dx.doi.org/10.1002/ggge.20136.

Hilairet, N., Reynard, B., Wang, Y., Daniel, I., Merkel, S., Nishiyama, N., Petitgirard, S., 2007. High-pressure creep of serpentinites, interseismic deformation, and initiation of subduction. Science 318, 1910–1913.

Hirose, H., Obara, K., 2010. Recurrence behavior of short-term slow slip and correlated nonvolcanic tremor episodes in western Shikoku, southwest Japan. J. Geophys. Res 115 (B00A21). http://dx.doi.org/10.1029/2008JB006050.

Husker, A.L., Kostoglodov, V., Cruz-Atienza, V.M., Legrand, D., Shapiro, N.M., Payero, J.S., Campillo, M., Huesca-Pérez, E., 2012. Temporal variations of non-volcanic tremor (NVT) locations in the Mexican subduction zone: finding the NVT sweet spot. Geochem. Geophys. Geosyst. 13 (Q03011). http://dx.doi.org/10.1029/2011GC003916.

Hyndman, R.D., Peacock, S.M., 2003. Serpentinization of the forearc mantle. Earth Planet. Sci. Lett. 212, 417–432.

Hyndman, R.D., McCrory, P.A., Wech, A., Kao, H., Ague, J., 2015. Cascadia subducting plate fluids channelled to fore-arc mantle corner: ETS and silica deposition. J. Geophys. Res. 120, 4344–4358.

Ide, S., 2012. Variety and spatial heterogeneity of tectonic tremor world-wide. J. Geophys. Res. 117 (B03302). http://dx.doi.org/10.1029/2011JB008840.

Idehara, K., Yabe, S., Ide, S., 2014. Regional and global variations in the temporal clustering of tectonic tremor activity. Earth, Planets and Space 66. http://dx.doi.org/10.1186/1880-5981-66-66.

Ito, Y., Obara, K., 2006. Dynamic deformation of the accretionary prism excites very low frequency earthquakes. Geophys. Res. Lett. 33 (L02311). http://dx.doi.org/10.1029/2005GL025270.

Janiszewski, H.A., Abers, G.A., 2015. Imaging the plate interface in the Cascadia seismogenic zone: new constraints from offshore receiver functions. Seismol. Res. Lett. 86. http://dx.doi.org/10.1785/0220150104.

Jiang, Y., Wdowinski, S., Dixon, T.H., Hackl, M., Protti, M., Gonzalez, V., 2012. Slow slip events in Costa Rica detected by continuous GPS observations, 2002-2011. Geochem. Geophys. Geosyst. 13 (Q04006).

Kanamori, H., Stewart, G.S., 1979. A slow earthquake. Phys. Earth Planet. Inter. 18, 167–175.

Kao, H., Shan, S.-J., Dragert, H., Rogers, G., 2009. Northern Cascadia episodic tremor and slip: a decade of tremor observations from 1997 to 2007. J. Geophys. Res. 114 (B00A12). http://dx.doi.org/10.1029/2008JB006046.

Kao, H., Shan, S.-J., Dragert, H., Rogers, G., Cassidy, J.F., Ramachandran, K., 2005. A wide depth distribution of seismic tremors along the northern Cascadia margin. Nature 436, 841–844.
Kao, H., Shan, S.-J., Dragert, H., Rogers, G., Cassidy, J.F., Wang, K., James, T.S., Ramachandran, K., 2008. Spatial–temporal patterns of seismic tremors in northern Cascadia. J. Geophys. Res. 111.
Katayama, I., Hirauchi, K.-I., Michibayashi, K., Ando, J.-I., 2009. Trench-parallel anisotropy produced by serpentine deformation in the hydrated mantle wedge. Nature 461, 1114–1117.
Katayama, I., Terada, T., Okazaki, K., Tanikawa, W., 2012. Episodic tremor and slow slip potentially linked to permeability contrasts at the Moho. Nat. Geosci. 5, 731–734.
Kato, A., Iidaka, T., Ikuta, R., Yoshida, Y., Katsumata, K., Iwasaki, T., Sakai, S.I., Thurber, C., Tsumura, N., Yamaoka, K., Watan- abe, T., Kunitomo, T., Yamazaki, F., Okubo, M., Suzuki, S., Hi-rata, N., 2010. Variations of fluid pressure within the subducting oceanic crust and slow earthquakes. Geophys. Res. Lett. 37 (L14310).
Kim, M.J., Schwartz, S.Y., Bannister, S., 2011. Non-volcanic tremor associated with the March 2010 Gisborne slow slip event at the Hikurangi subduction margin, New Zealand. Geophys. Res. Lett. 38 (L14301). http://dx.doi.org/10.1029/2011GL048400.
Kim, Y., Abers, G.A., Li, J., Christensen, D., Calkins, J., Rondenay, S., 2014. Alaska Megathrust 2: imaging the megathrust zone and Yakutat/Pacific plate interface in the Alaska subduction zone. J. Geophys. Res. 119. http://dx.doi.org/10.1002/2013JB010581.
Kim, Y., Clayton, R.W., Asimow, P.D., Jackson, J.M., 2013. Generation of talc in the mantle wedge and its role in subduction dynamics in central Mexico. Earth Planet. Sci. Lett. 384, 81–87. http://dx.doi.org/10.1016/j.epsl.2013.10.006.
Kim, Y., Clayton, R.W., Jackson, J.M., 2010. Geometry and seismic properties of the subducting Cocos plate in central Mexico. J. Geophys. Res. 115 (B06310). http://dx.doi.org/10.1029/2009JB006942.
Kim, Y., Miller, M.S., Pearce, F.D., Clayton, R.W., 2012. Seismic imaging of the Cocos plate subduction zone system in central Mexico. Geochem. Geophys. Geosyst. 13 (Q07001). http://dx.doi.org/10.1029/2012GC004033.
Kitajima, H., Saffer, D.M., 2012. Elevated pore pressure and anomalously low stress in regions of low frequency earthquakes along the Nankai Trough subduction megathrust. Geophys. Res. Lett. 39 (L23301). http://dx.doi.org/10.1029/2012GL053793.
Kodaira, S., Iidaka, T., Kato, A., Park, J.-O., Iwassaki, T., Kaneda, Y., 2004. High pore fluid pressure may cause silent slip in the Nankai Trough. Science 304, 1295–1298. http://dx.doi.org/10.1126/science.1096535.
Kostoglodov, V., Huster, A., Shapiro, N.M., Payero, J.S., Campillo, M., Cotte, N., Clayton, R., 2010. The 2006 slow slip event and nonvolcanic tremor in the Mexican subduction zone. Geophys. Res. Lett. 37 (L24301). http://dx.doi.org/10.1029/2010GL045424.
Kostoglodov, V., Singh, S.K., Santiago, J.A., Franco, S.I., Larson, K.M., Lowry, A.R., Bilham, R., 2003. A large silent earthquake in the Guerrero seismic gap, Mexico. Geophys. Res. Lett. 30, 1807.
Langston, C.A., 1977. Corvallis, Oregon, crustal and upper mantle receiver structure from teleseismic P and S waves. Bull. Seismol. Soc. Am. 67, 713–724.
Langston, C.A., 1981. Evidence for the subducting lithosphere under southern Vancouver Island and western Oregon from teleseismic P wave conversion. J. Geophys. Res. 86, 3857–3866.
Larson, K., Kostoglodov, V., Miyazaki, S., Santiago, J.A.S., 2007. The 2006 aseismic slow slip event in Guerrero, Mexico: new results from GPS. Geophys. Res. Lett. 34 (L13309). http://dx.doi.org/10.1029/2007GL029912.
Larson, K.M., Lowry, A.R., Kostoglodov, V., Hutton, W., Sanchez, O., Hudnut, K., Suarez, G., 2004. Crustal deformation measurements in Guerrero, Mexico. J. Geophys. Res. 109, B04409. http://dx.doi.org/10.1029/2003JB002843.
Lay, T., Kanamori, H., Ammon, C.J., Koper, K.D., Hutko, A.R., Ye, L., Yue, H., Rushing, T.M., 2012. Depth-varying rupture properties of subduction zone megathrust faults. J. Geophys. Res. 117 (B04311). http://dx.doi.org/10.1029/2011JB009133.
Li, J., Abers, G.A., Kim, Y.H., Christensen, D., 2013. Alaska megathrust 1: seismicity 43 years after the great 1964 Alaska megathrust earthquake. J. Geophys. Res. 118, 4861–4871. http://dx.doi.org/10.1002/jgrb.50358.
Linde, A.T., Gladwin, M.T., Johnston, M.J.S., Gwyther, R.L., Bilham, R.B., 1996. A slow earthquake sequence on the San Andreas fault. Nature 383, 65–68.
Linkimer, L., Beck, S.L., Schwartz, S.Y., Zandt, G., Levin, V., 2010. Nature of crustal terranes and the Moho in northern Costa Rica from receiver function analysis. Geochem. Geophys. Geosyst. 11. http://dx.doi.org/10.1029/2009GC002795.
Liu, Y., Rice, J.R., 2007. Spontaneous and triggered aseismic deformation transients in a subduction fault model. J. Geophys. Res. 112 (B09404).
Liu, Y., Rice, J.R., 2009. Slow slip prediction based on gabbro friction data compared to GPS measurements in northern Cascadia. J. Geophys. Res. 114 (B09407). http://dx.doi.org/10.1029/2008JB006142.
Lowry, A.R., 2006. Resonant slow fault slip in subduction zones forced by climatic load stress. Nature 442, 802–805. http://dx.doi.org/10.1038/nature05055.
Lowry, A.R., Larson, K.M., Kostoglodov, V., Bilham, R., 2001. Transient fault slip in Guerrero, southern Mexico. Geophys. Res. Lett. 28, 3753–3756.
MacKenzie, L.S., Abers, G.A., Rondenay, S., Fischer, K.M., 2010. Imaging a steeply dipping subducting slab in Southern Central America. Earth Planet. Sci. Lett. 296, 459–468.
Malservisi, R., Schwartz, S.Y., Voss, N., Protti, M., Gonzalez, V., Dixon, T.H., Jiang, Y., Newman, A.V., Richardson, J., Walter, J.I., Voyenko, D., 2015. Multiscale postseismic behavior on a megathrust: the 2012 Nicoya earthquake, Costa Rica. Geochem. Geophys. Geosyst. 16. http://dx.doi.org/10.1002/2015GC005794.
Manea, V.C., Manea, M., 2011. Flat-slab thermal structure and evolution beneath central Mexico. Pure Appl. Geophys. 168, 1475–1487. http://dx.doi.org/10.1007/s00024-010-0207-9.
Manning, C.E., 1994. The solubility of quartz in H_2O in the lower crust and upper mantle. Geochim. Cosmochim. Acta 58, 4831–4839.
McCaffrey, R., Wallace, L.M., Beavan, J., 2008. Slow slip and frictional transion at low temperatore at the Hikurangi subduction zone. Nature Geoscience 1, 316–320. http://dx.doi.org/10.1038/ngeo178.
McGary, R.S., Evans, R.L., Wannamaker, P.E., Elsenbeck, J., Rondenay, S., 2014. Pathway from subducting slab to surface for melt and fluids beneath Mount Rainier. Nature 511, 338–340.
Meneghini, F., di Toro, G., Rowe, C.D., Moore, J.C., Tsutsumi, A., Yamaguchi, A., 2010. Record of mega-earthquakes in subduction thrusts: the black fault rocks of Pasagshak Point (Kodiak Island, Alaska). Geol. Soc. Am. Bull. 122, 1280–1297. http://dx.doi.org/10.1130/B30049.1.
Miller, M.M., Melbourne, T.I., Johnson, D.J., Summer, W.Q., 2002. Periodic slow earthquakes from the Cascadia subduction zone. Science 295, 2423.
Miyazaki, S., Segall, P., McGuire, J.J., Kato, T., Hatanaka, Y., 2006. Spatial and temporal evolution of stress and slip rate during the 2000 Tokai slow earthquake. J. Geophys. Res. 111 (B03409). http://dx.doi.org/10.1029/2004JB003426.
Nabelek, J., Trehu, A., Li, X.Q., Fabritius, A., 1996. Lithospheric structure of the Cascadia Arc beneath Oregon. Eos Trans. AGU (Fall Meeting Supplement Abstract T72B-10).
Nadeau, R.M., Dolenc, D., 2005. Nonvolcanic tremors deep beneath the San Andreas Fault. Science 307, 389. http://dx.doi.org/10.1126/science.1107142.
Newman, A.V., Schwartz, S.Y., Gonzalez, V., DeShon, H.R., Protti, J.M., Dorman, L.M., 2002. Along-strike variability in the updip limit of the seismogenic zone below Nicoya Peninsula, Costa Rica. Geophys. Res. Lett. 29, 1977.
Nicholson, T., Bostock, M.G., Cassidy, J.F., 2005. New constraints on subduction zone structure in northern Cascadia. Geophys. J. Int. 161, 849–859.
Nikulin, A., Levin, A., Park, J., 2009. Receiver function study of the Cascadia megathrust: evidence for localized serpentinization. Geochem. Geophys. Geosyst. 10 (Q07004).
Obara, K., 2002. Nonvolcanic deep tremor associated with subduction in southwest Japan. Science 296 (5573), 1679–1681. http://dx.doi.org/10.1126/science.1070378.
Obara, K., 2011. Characteristics and interactions between non-volcanic tremor and related slow earthquakes in the Nankai subduction zone, southwest Japan. J. Geodyn. 52, 229–248.
Ohta, Y., Freymueller, J.T., Hreinsdottir, S., Suito, H., 2006. A large slow slip event and the depth of the seismogenic zone in the South Central Alaska subduction zone. Earth Planet. Sci. Lett. 247, 108–116. http://dx.doi.org/10.1016/j.epsl.2006.05.013.
Outerbridge, K.C., Dixon, T.H., Schwartz, S.Y., Walter, J.I., Protti, M., Gonzalez, V., Biggs, J., Thorwart, M., Rabbel, W., 2010. A tremor and slip event on the Cocos-Caribbean subduction zone as measured by a global positioning system (GPS) and seismic network on the Nicoya Peninsula, Costa Rica. J. Geophys. Res. 115 (B10408). http://dx.doi.org/10.1029/2009JB006845.
Pardo, M., Suarez, G., 1995. Shape of the subducted Rivera and Cocos plates in southern Mexico: seismic and tectonic implications. J. Geophys. Res. 100, 12,357–12,373.
Payero, J.S., Kostoglodov, V., Shapiro, N., Mikumo, T., Iglesias, A., Pérez-Campos, X., Clayton, R.W., 2008. Nonvolcanic tremor observed in the Mexican subduction zone. Geophys. Res. Lett. 35 (L07305). http://dx.doi.org/10.1029/2007GL032877.
Peacock, S.M., 2009. Thermal and metamorphic environment of subduction zone episodic tremor and slip. J. Geophys. Res. 114, B00A07.
Peacock, S.M., Hyndman, R.D., 1999. Hydrous minerals in the mantle wedge and the maximum depth of subduction thrust earthquakes. Earth Planet. Sci. Lett. 26, 2517–2520.
Peacock, S.M., Wang, K., 1999. Seismic consequences of warm versus cool subduction metamorphism: examples from southwest and northeast Japan. Science 286 (5441), 937–939. http://dx.doi.org/10.1126/science.286.5441.937.
Peacock, S.M., Christensen, N.I., Bostock, M.G., Audet, P., 2011. High pore pressures and porosity at 35 km depth in the Cascadia subduction zone. Geology 39, 471–474.
Perez-Campos, X., Kim, Y., Husker, A., Davis, P.M., Clayton, R.W., Iglesias, A., Pacheco, J.F., Singh, S.K., Manea, V.C., Gurnis, M., 2008. Horizontal subduction and truncation of the Cocos Plate beneath central Mexico. Geophys. Res. Lett. 35, 18.
Peterson, C.L., Christensen, D.H., 2009. Possible relationship between nonvolcanic tremor and the 1998-2001 slow slip event, South Central Alaska. J. Geophys. Res. 114 (B06302). http://dx.doi.org/10.1029/2008JB006096.
Piana Agostinetti, N., Miller, M.S., 2014. The fate of the downgoing oceanic plate: insight from the Northern Cascadia subduction zone. Earth Planet. Sci. Lett. 408, 237–251.
Plafker, G., Moore, J.C., Winkler, G.R., 1994. Geology of the southern Alaska margin. In: Plafker, G., Berg, H.C. (Eds.), The Geology of Alaska. Vol. G1. Geological Society of America Bulletin, Boulder, CO., pp. 384–449.
Plourde, A.P., Bostock, M.G., Audet, P., Thomas, A.M., 2015. Low-frequency earthquakes at the southern Cascadia margin. Geophys. Res. Lett. 42, 4849–4855.
Radiguet, M., Cotton, F., Vergnolle, M., Camppillo, M., Valette, B., Kostoglodov, V., Cotte, N., 2011. Spatial and temporal evolution of a long term slow slip event: the 2006 Guerreo slow slip event. Geophys. J. Int. 184, 816–828. http://dx.doi.org/10.1111/j.1365-246X.2010.04866.x.
Reyners, M., Eberhart-Phillips, D., Stuart, G., Nishimura, Y., 2006. Imaging subduction from the trench to 300 km depth beneath the central North Island, New Zealand, with *Vp* and *Vp/Vs*. Geophys. J. Int. 165, 565–583. http://dx.doi.org/10.1111/j.1365-246X.2006.02897.x.
Rogers, G., Dragert, H., 2003. Episodic tremor and slip on the Cascadia subduction zone: the chatter of silent slip. Science 300, 1942–1943.
Rondenay, S., Abers, G.A., van Keken, P.E., 2008. Seismic imaging of subduction zone metamorphism. Geology 36, 275–278.
Rondenay, S., Bostock, M.G., Shragge, J., 2001. Multiparameter two-dimensional inversion of scattered teleseismic body waves: 3—application to the Cascadia 1993 data set. J. Geophys. Res. 106, 30795–30807.
Royer, A.A., Bostock, M.G., 2014. A comparative study of low frequency earthquake templates in northern Cascadia. Earth Planet. Sci. Lett. 402, 247–256.
Royer, A.A., Thomas, A.M., Bostock, M.G., 2015. Tidal modulation and triggering of low-frequency earthquakes in northern Cascadia. J. Geophys. Res. 120, 384–405.

Rubin, A.M., 2008. Episodic slow slip events and rate-and-state friction. J. Geophys. Res. 113 (B11414).
Rubin, A.M., Armbruster, J.G., 2013. Imaging slow-slip front in Cascadia with high precision cross-station tremor locations. Geochem. Geophys. Geosyst. 14, 5371–5392. http://dx.doi.org/10.1002/2013GC005031.
Rubinstein, J.L., La Rocca, M., Vidale, J.E., Creager, K.C., Wech, A.G., 2008. Tidal modulation of non-volcanic tremor. Science 319, 186–189.
Rubinstein, J.L., Shelly, D.R., Ellsworth, W., 2010. Non-Volcanic Tremor: A Window into the Roots of Fault Zones. In: CLoetingh, S., Negendank, J. (Eds.), New Frontiers in Integrated Solid Earth Sciences. Springer, Dordrecht, pp. 287–314.
Rubinstein, J.L., Vidale, J.E., Gomberg, J., Bodin, P., Creager, K.C., Malone, S.D., 2007. Non-volcanic tremor driven by large transient shear stresses. Nature 448, 579–582.
Saffer, D.M., Wallace, L.M., 2015. The frictional, hydrologic, metamorphic and thermal habitat of shallow slow earthquakes. Nat. Geosci. 8, 594–600. http://dx.doi.org/10.1038/ngeo2490.
Schwartz, S.Y., Rokosky, J.M., 2007. Slow Slip Events and Seismic Tremor at Circum-Pacific Subduction Zones. Rev. of Geophys 45 (RG3004). http://dx.doi.org/10.1029/2006RG000208.
Scholz, C.H., 1998. Earthquakes and friction laws. Nature 391, 37–42.
Segall, P., Rubin, A.M., Bradley, A.M., Rice, J.R., 2010. Dilatant strengthening as a mechanism for slow slip events. J. Geophys. Res. 115 (B12305).
Shelly, D.R., Beroza, G.C., Ide, S., 2006. Low-frequency earthquakes in Shikoku, Japan, and their relationship to episodic tremor and slip. Nature 442, 188–191. http://dx.doi.org/10.1038/nature04931.
Shelly, D.R., Beroza, G.C., Ide, S., 2007. Non-volcanic tremor and low frequency earthquake swarms. Nature 446, 305–307. http://dx.doi.org/10.1038/nature05666.
Shen, Z.K., Wang, Q., Bürgmann, R., Wan, Y., 2005. Pole-tide modulation of slow slip events at circum-Pacific subduction zones. Bull. Seismol. Soc. Am. 95, 2009–2015.
Shiomi, K., Park, J., 2008. Structural features of the subducting slab beneath the Kii Peninsula, central Japan: seismic evidence of slab segmentation, dehydration, and anisotropy. J. Geophys. Res. 113 (B10318). http://dx.doi.org/10.1029/2007JB005535.
Song, T.A., Kim, Y., 2012. Localized seismic anisotropy associated with long-term slow-slip events beneath southern, Mexico. Geophys. Res. Lett. 39 (L09308). http://dx.doi.org/10.1029/2012GL051324.
Song, T.A., Helmberger, D.V., Brudzinski, M.R., Clayton, R.W., Davis, P., Perez-Campos, X., Singh, S.K., 2009. Subducting slab ultraslow velocity layer conincident with silent earthquake in southern Mexico. Science 324, 502–506.
Soyer, W., Unsworth, M., 2006. Deep electrical structure of the northern Cascadia (British Columbia, Canada) subduction zone: implications for the distribution of fluids. Geology 34, 53–56.
Syracuse, E.M., van Keken, P.E., Abers, G.A., 2010. The global range of subduction zone thermal models. Phys. Earth Planet. Inter. 183, 73–90.
Szeliga, W., Melbourne, T., Santillan, M., Miller, M., 2008. GPS constraints on 34 slow slip events within the Cascadia subduction zone, 1997–2005. J. Geophys. Res. 113 (B04404).
Thomas, A.M., Bostock, M.G., 2015. Identifying low-frequency earthquakes in central Cascadia using cross-station correlation. Tectonophysics 658, 111–116.
Toomey, D.R., Allen, R.M., Barclay, A.H., Bell, S.W., Bromirski, P.D., Carlson, R.L., Chen, X., Collins, J.A., Dziak, R.P., Evers, B., Forsyth, D.W., Gerstoft, P., Hooft, E.E.E., Livelybrooks, D., Lodewyk, J.A., Luther, D.S., McGuire, J.J., Schwartz, S.Y., Tolstoy, M., Tréhu, A.M., Weirathmueller, M., Wilcock, W.S.D., 2014. The Cascadia initiative: a sea change in seismological studies of subduction zones. Oceanography 27 (2), 138–150. http://dx.doi.org/10.5670/oceanog.2014.49.
Vannucchi, P.F., Sage, J., Phipps Morgan, J., Remiti, F., Collot, J.-Y., 2012. Toward a dynamic concept of the subduction channel at erosive convergent margins with implications for interpolate material transfer. Geochem. Geophys. Geosyst. 13 (Q02003). http://dx.doi.org/10.1029/2011GC003846.
Vergnolle, M., Walpersdorf, A., Kostoglodov, V., Tregoning, P., Santiago, J.A., Cotte, N., Franco, S.I., 2010. Slow slip events in Mexico revised from the processing of 11 years GPS observations. J. Geophys. Res. 115 (B08403). http://dx.doi.org/10.1029/2009JB006852.
von Huene, R., Weinrebe, W., 2012. Subducting plate geology in three great earthquake ruptures of the western Alaska margin, Kodiak to Unimak. Geosphere 8 (3), 628–644. http://dx.doi.org/10.1130/GES00715.1.
von Huene, R., Klaeschen, D., Gutscher, M., Fruehn, J., 1998. Mass and fluid flux during accretion at the Alaskan margin. Geol. Soc. Am. Bull. 110 (4), 468–482.
Wada, I., Wang, K., He, J., Hyndman, R.D., 2008. Weakening of the subduction interface and its effects on surface heat flow, slab dehydration, and mantle wedge serpentinization. J. Geophys. Res. 113. http://dx.doi.org/10.1029/2007JB005190.
Wallace, L.M., Beavan, J., 2010. Diverse slow slip behavior at the Hikurangi subduction margin, New Zealand. J. Geophys. Res. 115 (B12402). http://dx.doi.org/10.1029/2010JB007717.
Wallace, L.M., Eberhart-Phillips, D., 2013. Newly observed, deep slow slip events at the central Hikurangi margin, New Zealand: implications for downdip variability of slow slip and tremor, and relationship to seismic structure. Geophys. Res. Lett. 40, 5393–5398. http://dx.doi.org/10.1002/2013GL057682.
Wallace, L.M., Beavan, J., McCaffrey, R., Darby, D., 2004. Subduction zone coupling and tectonic block rotations in the North Island, New Zealand. J. Geophys. Res. 109 (B12406). http://dx.doi.org/10.1029/2004JB003241.
Walter, J.I., Schwartz, S.Y., Protti, M., Gonzalez, V., 2011. Persistent tremor within the northern Costa Rica seismogenic zone. Geophys. Res. Lett. 38 (L01307).
Walter, J.I., Schwartz, S.Y., Protti, M., Gonzalez, V., 2013. The synchronous occurence of shallow tremor and very low frequency earthquakes offshore of the Nicoya Peninsula, Costa Rica. Geophys. Res. Lett. 40, 1517–1522.
Wang, X.-Q., Schubnel, A., Fortin, J., David, E.C., Gueguen, Y., Ge, H.-K., 2012. High Vp/Vs ratio: saturated cracks or anisotropy effects? Geophys. Res. Lett. 39 (L11307). http://dx.doi.org/10.1029/2012GL051742.
Wech, A.G., Creager, K.C., 2011. A continuum of stress, strength and slip in the Cascadia subduction zone. Nat. Geosci. 4, 624–628.
Wech, A.G., Creager, K.C., Melbourne, T.I., 2009. Seismic and geodetic constraints on Cascadia slow slip. J. Geophys. Res. 114 (B10316).
Wei, M., McGuire, J.J., Richardson, E., 2012. A slow slip event in the South Central Alaska subduction zone and related seismicity anomaly. Geophys. Res. Lett. 39 (L15309). http://dx.doi.org/10.1029/2012GL052351.
Yabe, S., Ide, S., Yoshioka, S., 2014. Along-strike variations in temperature and tectonic tremor activity along the Hikurangi subduction zone, New Zealand. Earth Planets Space 66, 142. http://dx.doi.org/10.1186/s40623-014-0142-6.
Yoshioka, S., Mikumo, T., Kostoglodov, V., Larson, K.M., Lowry, A.R., Singh, S.K., 2004. Interplate coupling and a recent aseismic slow slip event in the Guerrero seismic gap of the Mexican subduction zone, as deduced from GPS data inversion using a Bayeseian information criterion. Phys. Earth Planet. Inter. 146, 513–530. http://dx.doi.org/10.1016/j.pepi.2004.05.006.
Yue, H., Lay, T., Schwartz, S.Y., Rivera, L., Protti, M., Dixon, T.H., Owen, S., Newman, A.V., 2013. The 5 September 2012 Nicoya, Costa Rica M_w 7.6 earthquake rupture process from joint inversion of high-rate GPS, strong-motion, and teleseismic P wave data and its relationship to adjacent plate boundary interface properties. J. Geophys. Res. 118, 5453–5466.
Zweck, C., Freymueller, J.T., Cohen, S.C., 2002. Three-dimensional elastic dislocation modeling of the postseismic response to the 1964 Alaska earthquake. J. Geophys. Res. 107 (B4). http://dx.doi.org/10.1029/2001JB000409.